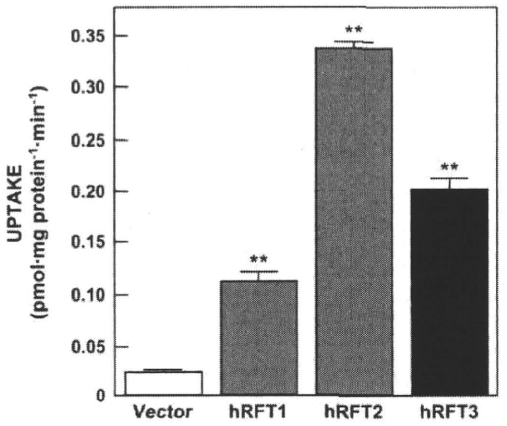

FIGURE 1 Uptake of [^{3}H]riboflavin by HEK293 cells transfected with empty vector, hRFT1, hRFT2, and hRFT3. The cells were incubated in buffer (pH 7.4) containing 5 nmol/L [^{3}H]riboflavin for 1 min at 37°C. Each bar represents the mean ± SEM, n = 3. **Different from vector-transfected cells, $P < 0.01$.

therefore indicated to be the first member of a novel mammalian riboflavin transporter RFT family.

Thereafter, the second member RFT2 was also identified as a homolog of RFT1 (8). hRFT2 shows 42.9% amino acid identity with hRFT1. hRFT1 mRNA was strongly expressed in the placenta and small intestine, whereas rRFT2 mRNA was strongly expressed in the testis and small intestine (3,8). Based on these results, RFT1 and RFT2 were suggested to play important roles in intestinal riboflavin absorption. After absorption, riboflavin is distributed from the blood to several tissues and utilized as a coenzyme in metabolic reactions. Yet in some tissues, such as brain and liver, RFT1 and RFT2 were only slightly expressed. Therefore, another member belonging to the RFT family could play a key role in riboflavin handling.

In this study, we successfully isolated hRFT3 as a new member of the RFT gene family. hRFT3 mRNA was strongly expressed in the brain. Because the functional characteristics of hRFT1 and hRFT2 had not been clearly demonstrated, we compared functional characteristics of hRFT3 with those of hRFT1 and hRFT2.

Materials and Methods

Isolation of hRFT3. We searched for the human homolog of hRFT1 in the GenBank database by using the BLASTN algorithm and found GPR 172A (GenBank accession no. NM_024531) as well as hRFT2. The molecular function of GPR172A has yet to be determined. We designated it hRFT3 (GenBank accession no. AB522904) based on its functional characterization as shown below. In addition, we also searched for the rat ortholog, but no clone was identified except for rRFT1 and rRFT2. The hRFT3 cDNA was isolated by RT-PCR with the forward primer 5′-GGAAGCTTGCCCTAGGTGGGAAAAGAAC-3′ and the reverse primer 5′-GGTCTAGAGAGGGAAAGACAGGTGTTGG-3′ using human small intestine-derived total RNA commercially purchased from Clontech. The PCR was performed using PrimeSTAR HS DNA Polymerase (TAKARA BIO) according to the following profile: 98°C for 10 s, 52°C for 5 s, 72°C for 2.5 min, 36 cycles. The hRFT2 cDNA was isolated similarly using hRFT2-specific primers designed based on the sequence in GenBank (accession no. NM_033409). The primers were as follows: forward primer 5′-GGAAGCTTCAGTCCAGATCCCAGGAGAG-3′ and reverse primer 5′-GGCTCGAGGGAGATCTGAGCTGGTCGTC-3′. PCR products were subcloned into the expression vector pcDNA3.1/Hygro(+) (Life Technologies) or pEnhanced Green Fluorescent Protein (EGFP)-C1 (Clontech) and sequenced using a 96-capillary 3730xl DNA Analyzer (Life Technologies).

The hRFT1 cDNA was previously isolated and subcloned into the expression vector pBK-CMV (Stratagene) (3). It was amplified by PCR with the hRFT1 plasmid using hRFT1-specific following primers designed based on the sequence in GenBank (accession no. AB362533): forward primer 5′-GGAAGCTTTTCCAGAAGAGCCAAAGCAT-3′ and reverse primer 5′-GGTCTAGAGCCTCACGATGAAGACAGGT-3′ and it was subcloned into the expression vector pcDNA3.1/Hygro(+) or pEGFP-C1. Multiple sequence alignments and phylogenic trees were produced using GENETYX-MAC version 13 (Software Development).

Cell culture and transfection. Human embryonic kidney (HEK)293 cells (American Type Culture Collection CRL-1573) were cultured in the complete medium consisting of DMEM (Wako Pure Chemical Industries) supplemented with 10% fetal bovine serum (Life Technologies) in an atmosphere of 5% CO_2-95% air at 37°C.

For a transient expression system, pcDNA3.1/Hygro(+) and pEGFP-C1 containing hRFT1, hRFT2, and hRFT3 were purified using the Hispeed Plasmid Purification system (QIAGEN K.K) and Wizard Plus SV Minipreps DNA Purification system (Promega), respectively. On the day before transfection, cells were seeded onto poly-D-lysine–coated 24-well plates (Becton, Dickinson and Company) at a density of 7.5×10^4 cells/well for the uptake experiment, poly-D-lysine/laminin–coated 4-well culture slide (Becton, Dickinson and Company) at a density of 2.0×10^5

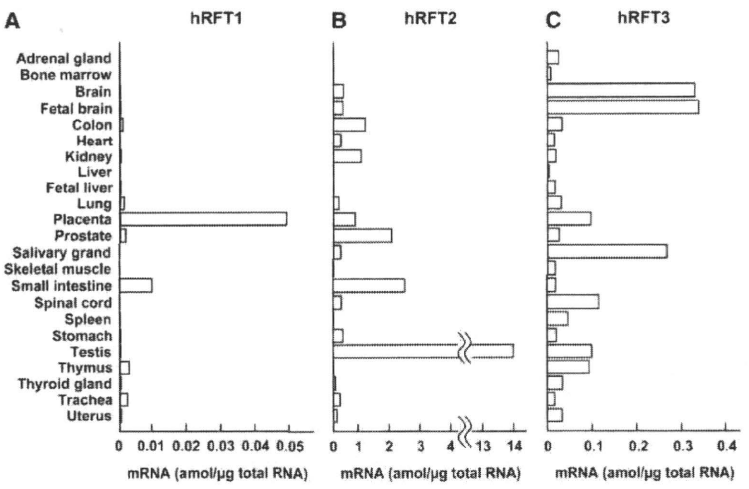

FIGURE 2 Real-time PCR analysis of various human tissues for hRFT1 (*A*), hRFT2 (*B*), and hRFT3 (*C*). Total RNA of various human tissues was reverse-transcribed to yield cDNA.

cells/well for fluorescence chemistry, and 60-mm tissue culture dish (Asahi Glass) at a density of 2.0×10^6 cells/dish for Western blot analysis. The cells were transfected with 0.2 μg of plasmid DNA using 1 μL of Lipofectamine 2000 Reagent (Life Technologies) per well for the uptake experiment, 0.8 μg of plasmid DNA using 2 μL of Lipofectamine 2000 Reagent per well for fluorescence chemistry, and 8 μg of plasmid DNA using 20 μL of Lipofectamine 2000 Reagent for Western blot analysis according to the manufacturer's instructions. Forty-eight hours after transfection, the cells were used for subsequent experiments.

Real-time PCR. Total RNA (1 μg) from various human tissues was commercially purchased from Clontech and reverse-transcribed to yield cDNA. To determine the sum of the mRNA expression of hRFT1, hRFT2, and hRFT3, real-time PCR was performed with an ABI PRISM 7700 sequence detector (Life Technologies). Real-time PCR was carried out in a total volume of 20 μL containing 5 μL of cDNA sample, 2 μL of TaqMan Gene Expression assays, and 10 μL of TaqMan Universal Master mix (Life Technologies). The starting mRNA copy number of the target sequence was established by determining the fractional PCR threshold cycle number at which a fluorescence signal generated during the replication process passed above a threshold value. The initial amount of target mRNA in each sample was estimated from the experimental threshold cycle value with a standard curve generated using known amounts of standard plasmid DNA. Real-time PCR conditions were as follows: 95°C for 15 s, 60°C for 60 s, 50 cycles. TaqMan Gene Expression assays were purchased from Life Technologies: hRFT1, Hs01079030_gl; hRFT2, Hs00364295_ml; hRFT3, Hs01859203_sl.

Fluorescence cytochemistry. HEK293 cells were transfected with the plasmid vector pEGFP-C1 containing hRFT1, hRFT2, and hRFT3 as described above. The cells were fixed with 2% paraformaldehyde for 10 min at room temperature and observed using a BIOREVO BZ-9000 fluorescence microscope (KEYENCE).

Western blot analysis. Western blot analysis was carried out using a NuPAGE electrophoresis system (Life Technologies) as described previously with some modifications (9). Briefly, cells were homogenized by sonication in buffer (250 mmol/L sucrose and 5 mmol/L HEPES, pH 7.4) and were then centrifuged at 2000 × *g* for 10 min. The supernatant was recentrifuged at 15,000 × g for 30 min and the pellet was used for the crude membrane samples. Crude membrane fractions (2.5 μg) were separated by NuPAGE 4–12% Bis-Tris gels, 1.0 mm, 12 well (Life Technologies), and were transferred onto 0.2 μm polyvinylidene difluoride membrane (Life Technologies) according to the manufacturer's instructions. Primary and secondary antibodies were anti-green fluorescent protein (Roche Diagnostics) and horseradish peroxidase-conjugated anti-mouse IgG (GE Healthcare Bio-Sciences), respectively. The bound antibody was detected on X-ray film using a Visualizer Spray and Glow ECL Western Blotting system (Millipore).

Uptake experiment. Cellular uptake of [^{3}H]riboflavin (0.903 TBq/mmol, Moravek Biochemicals) was measured with monolayer cultures grown on poly-D-lysine–coated 24-well plates. The experimental procedures were described previously (3,10). Briefly, the cells were preincubated with 0.2 mL of incubation buffer (pH 7.4) for 10 min at 37°C. The buffer was then removed and 0.2 mL of each incubation buffer containing 5 nmol/L [^{3}H] riboflavin was added. The buffer was aspirated at the end of the incubation period and the monolayers were rapidly washed twice with 1 mL of ice-cold incubation buffer. The cells were solubilized in 0.5 mL of 0.5 mol/L NaOH and then the radioactivity in aliquots was determined by liquid scintillation counting. The composition of incubation buffer was as follows: 145 mmol/L NaCl, 3 mmol/L KCl, 1 mmol/L $CaCl_2$, 0.5 mmol/L $MgCl_2$, 5 mmol/L D-glucose, and 5 mmol/L HEPES (pH 7.4 unless otherwise specified; pH was adjusted with NaOH). Na^+-free incubation buffer was prepared by replacing Na^+ with N-methyl-D-glucamine or choline (pH 7.4; pH was adjusted with HCl or KOH), and Cl^--free incubation buffer was prepared by replacing Cl^- with gluconate or sulfate (pH 7.4; pH was adjusted with NaOH). The protein content of the solubilized cells was determined by the method of Bradford with a Bio-Rad Protein Assay kit (Bio-Rad Laboratories) with bovine γ-globulin as a standard.

The specific uptake of [^{3}H]riboflavin by hRFT1, hRFT2, and hRFT3 was calculated by subtracting the uptake of [^{3}H]riboflavin by HEK293 cells transfected with empty vector from uptake with each hRFT. The concentration dependence of riboflavin transport was fit by the Michaelis-Menten equation: $V = V_{max}[S]/(K_m + [S])$, where V is the transport rate, V_{max} is the maximal transport rate, [S] is the concentration of riboflavin, and K_m is the Michaelis-Menten constant.

Statistical analysis. Data are expressed as the means ± SEM. Time dependence or concentration dependence of riboflavin transport was analyzed by 1-way ANOVA using GraphPad Prism (version 5.0b, GraphPad Software). Other data were analyzed by Dunnett's 2-tailed test after 1-way ANOVA. $P < 0.05$ was considered significant.

Results

Isolation of a new hRFT3. A single clone encoding hRFT3 was isolated and sequenced. The hRFT3 cDNA (GenBank accession no. AB522904) consists of 1451 bp with an open reading frame encoding a 445-amino acid protein. It was predicted to have 10 putative membrane-spanning domains by the SOSUI program

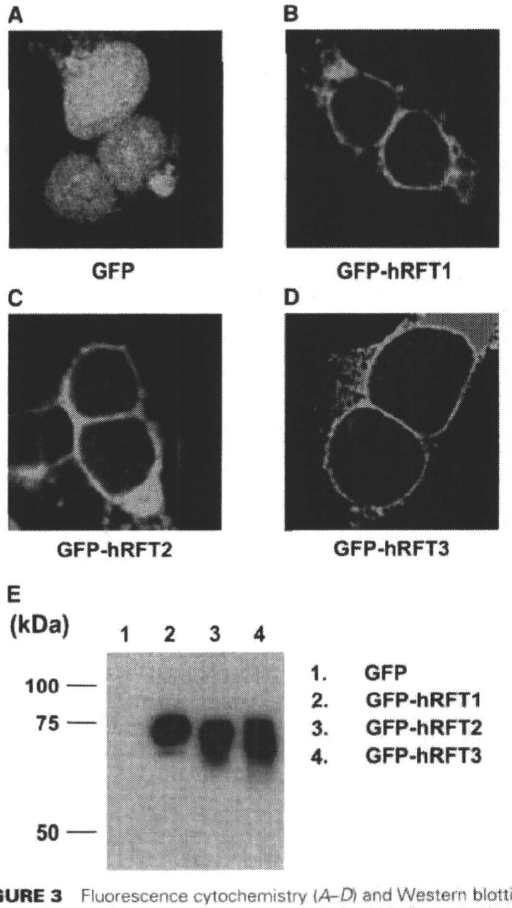

FIGURE 3 Fluorescence cytochemistry (*A–D*) and Western blotting (*E*) of EGFP-tagged empty vector, hRFT1, hRFT2, and hRFT3 introduced in HEK293 cells. Cells were fixed with 2% paraformaldehyde and observed using BIOREVO BZ-9000 fluorescence microscope. Western blot analysis was performed using the crude membrane of HEK293 cells expressing EGFP-tagged hRFT1, hRFT2, and hRFT3.

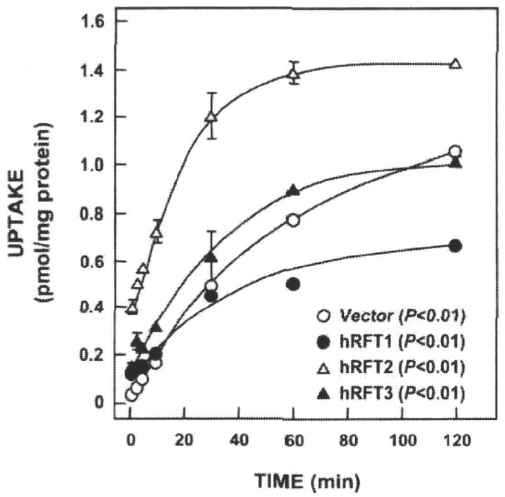

FIGURE 4 Time-dependent uptake of [^{3}H]riboflavin by HEK293 cells transfected with empty vector, hRFT1, hRFT2, and hRFT3. The cells were incubated in incubation buffer (pH 7.4) containing 5 nmol/L [^{3}H] riboflavin for various periods at 37°C. Each point represents the mean ± SEM, n = 3.

(4). hRFT3 shows 86.7% amino acid identity with hRFT1, 81.5% with rRFT1, 44.1% with hRFT2, and 43.1% with rRFT2. The amino acid sequences and phylogenic trees of hRFT3, hRFT1, rRFT1, hRFT2, and rRFT2 are shown in **Supplemental Figure 1**. The uptake of [^{3}H]riboflavin was significantly increased by transfection with hRFT3 as well as hRFT1 and hRFT2 (**Fig. 1**), indicating that hRFT3 is also a riboflavin transporter of the RFT family.

Tissue distribution and cellular localization of hRFT1, hRFT2, and hRFT3. The mRNA levels of hRFT1, hRFT2, and hRFT3 were examined by real-time PCR (**Fig. 2**). The hRFT1 mRNA was expressed in the placenta and small intestine. hRFT2 was primarily expressed in the testis and strongly in the small intestine and prostate. hRFT3 was strongly expressed in the brain, fetal brain, and salivary gland. To visualize the cellular localization of these proteins, EGFP-tagged hRFT1, hRFT2, and hRFT3 was introduced into HEK293 cells. Fluorescence was observed *in the plasma membrane* of the cells transfected with EGFP-tagged hRFT1, hRFT2, and hRFT3 (**Fig. 3***B–D*). In addition, Western blot analysis was carried out using the crude membrane of HEK293 cells transfected with these cDNA (Fig. 3*E*). A strong signal for EGFP-tagged hRFT1, hRFT2, and hRFT3 was detected.

Functional characterization of hRFT1, hRFT2, and hRFT3. We examined the uptake of [^{3}H]riboflavin by HEK293 cells transfected with empty vector, hRFT1, hRFT2, and hRFT3. The uptake of [^{3}H]riboflavin increased in a time-dependent manner (**Fig. 4**) and in a concentration-dependent manner (**Fig. 5***A*). The specific uptake by each hRFT was calculated (Fig. 5*B–D*). In addition, Eadie-Hofstee plots were constructed (Fig. 5*E–G*). The apparent K_m values of hRFT1, hRFT2, and hRFT3 for riboflavin were 1.38 ± 0.27, 0.98 ± 0.11, and 0.33 ± 0.07 μmol/L, respectively, and V_{max} values of these transporters were 12.2 ± 0.8, 63.8 ± 9.3, and 5.2 ± 0.7 pmol·mg protein^{-1}·min^{-1}, respectively. The replacement of Na^+ with N-methyl-D-glucamine or choline did not affect hRFT-mediated uptake of [^{3}H]riboflavin

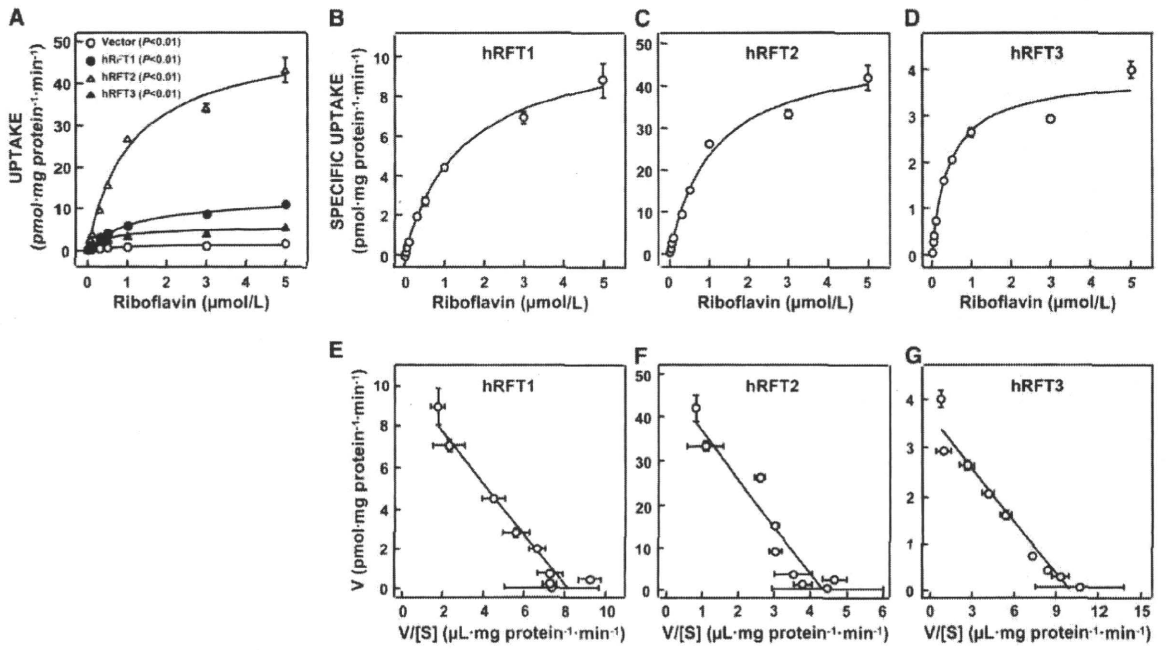

FIGURE 5 Concentration-dependent uptake of [^{3}H]riboflavin by HEK293 cells transfected with empty vector, hRFT1, hRFT2, and hRFT3 (*A*). The specific uptake of [^{3}H]riboflavin by hRFT1 (*B*), hRFT2 (*C*), and hRFT3 (*D*) was calculated by subtracting the uptake of [^{3}H]riboflavin by HEK293 cells transfected with empty vector from the uptake with hRFT. Eadie-Hofstee plots of the concentration-dependent uptake by each hRFT (*E–G*) are shown. The cells were incubated in buffer (pH 7.4) containing [^{3}H]riboflavin at various concentrations for 1 min at 37°C. Each point represents the mean ± SEM, n = 3.

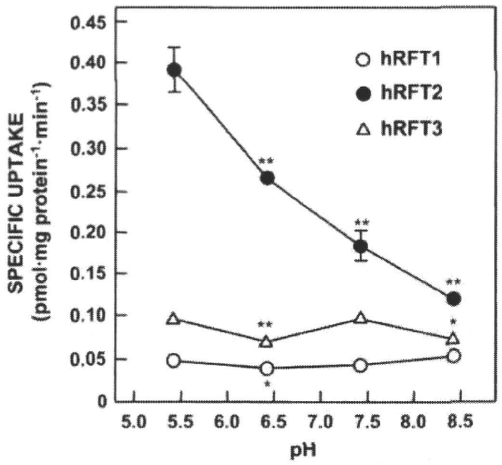

FIGURE 6 pH dependence of [^{3}H]riboflavin uptake by HEK293 cells transfected with hRFT1, hRFT2, and hRFT3. The specific uptake of [^{3}H]riboflavin by hRFT1, hRFT2, and hRFT3 was calculated by subtracting the uptake of [^{3}H]riboflavin by HEK293 cells transfected with empty vector from the uptake with hRFT family genes. The cells were incubated in buffer (pH 5.4–8.4) containing 5 nmol/L [^{3}H] riboflavin for 1 min at 37°C. Each point and bar represents the mean ± SEM, $n = 3$. Asterisks indicate different from cells incubated at pH 5.4: $^*P < 0.05$, $^{**}P < 0.01$.

(**Supplemental Fig. 2A**). Similarly, the replacement of Cl^- with gluconate or sulfate did not affect specific uptake by these transfectants (Supplemental Fig. 2*B*). We observed no pH dependence of hRFT1- and hRFT3-mediated uptake of [^{3}H] riboflavin (**Fig. 6**). The transport of [^{3}H]riboflavin by hRFT2, however, decreased as the extracellular pH was changed from 5.4 to 8.4. The chemical structures of riboflavin and its analogs are shown in **Figure 7***A*. The hRFT1-, hRFT2-, and hRFT3-mediated uptakes of [^{3}H]riboflavin were completely inhibited by excess unlabeled riboflavin and lumiflavine, whereas they were modestly inhibited by FMN (Fig. 7*B–D*). FAD slightly but significantly inhibited the hRFT3-mediated uptake of [^{3}H]riboflavin. D-Ribose, cimetidine, probenecid, thiamine, and folate only slightly and in several instances not significantly affected the specific uptake of [^{3}H]riboflavin by hRFT1, hRFT2, and hRFT3.

Discussion

In the present study, we identified hRFT3, which is a new member of the RFT gene family. The deduced amino acid sequence of hRFT3 shows 86.7 and 44.1% identity with hRFT1 and hRFT2, respectively (Supplemental Fig. 1). Based on their amino acid sequences, hRFT3 and hRFT1 were originally annotated as GPR172A (GenBank accession no. NM_024531) and GPR172B (GenBank accession no. NM_017986.2), respectively. However, their functional characteristics as GPR have not been demonstrated. They were predicted to have 10 putative membrane-spanning domains by the SOSUI program (4) and their riboflavin transport activity was indicated (Figs. 1, 4, 5). These results indicated that the GPR172 family could be designated as riboflavin transporter RFT family.

Interestingly, hRFT3 mRNA was predominantly expressed in the brain, whereas hRFT1 and hRFT2 mRNA were strongly expressed in the small intestine, but not brain (Fig. 2). The brain has developed specific carrier systems for the uptake of vital nutrients (e.g. glucose, amino acids, vitamins, and minerals), which are independent of intestinal transporters involved in absorption of the nutrients. For example, facilitative glucose transporter 1, rather than intestinal glucose transporter 2, plays a role in glucose uptake in the brain (11–13). In addition, brain-type sodium-dependent vitamin C transporter 2, but not intestinal sodium-dependent vitamin C transporter 1, is important for ascorbic acid homeostasis (14,15). In the case of riboflavin, a carrier-mediated mechanism also maintains riboflavin homeostasis in the brain (16–19). Thus, there is much interest in how hRFT3 works in the brain.

Previous studies demonstrated that the concentration of total riboflavin (riboflavin, FMN, and FAD) in the brain was 8.8 μmol/L, which was ~50 times higher than in plasma in adult rabbits (16,17). In addition, the concentrations of FMN and FAD in the brain remained relatively constant in severe deficiency as well as after high doses of riboflavin (18). It was also reported that

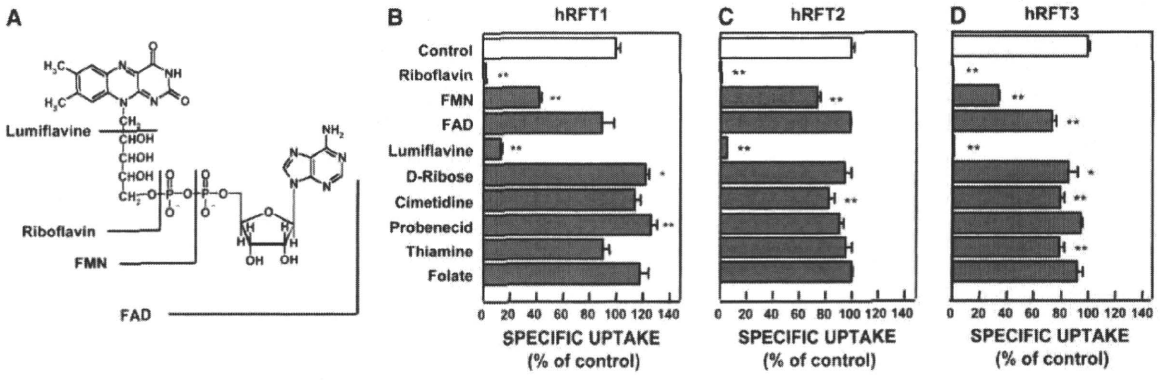

FIGURE 7 The chemical structure of riboflavin and its analogs (*A*) and the inhibitory effect of riboflavin analogs at 0.1 mmol/L and other inhibitors at 1.0 mmol/L on the specific uptake of [^{3}H]riboflavin by HEK293 cells transfected with hRFT1 (*B*), hRFT2 (*C*), and hRFT3 (*D*). The specific uptake of [^{3}H]riboflavin by hRFT1, hRFT2, and hRFT3 was calculated by subtracting the uptake of [^{3}H]riboflavin by HEK293 cells transfected with empty vector from the uptake with hRFT1, hRFT2, and hRFT3. The cells were incubated in buffer (pH 7.4) containing 5 nmol/L [^{3}H]riboflavin in the presence of inhibitors for 1 min at 37°C. Each bar represents the mean ± SEM, $n = 3$. Asterisks indicate different from control cells: $^*P < 0.05$, $^{**}P < 0.01$.

isolated rabbit brain slices contained a saturable accumulation system for riboflavin, which was inhibited by other flavins but not by D-ribose and probenecid (19). These previous reports indicated that the characteristics of riboflavin transport in the brain were similar to those of hRFT3 (Figs. 4, 5*D*, 7*D*). Therefore, hRFT3 would play an important role in the maintenance of riboflavin homeostasis in the brain.

Comparative functional characterization of hRFT1, hRFT2, and hRFT3 was carried out in this study and revealed some differences in the features of the hRFT family. hRFT1, hRFT2, and hRFT3 were independent of extracellular Na^+ and Cl^- (Supplemental Fig. 2*A*,*B*) and their substrate specificities were similar (Fig. 7*B–D*). On the other hand, the transport of riboflavin by hRFT1 and hRFT3 was independent of extracellular pH, whereas that by hRFT2 was sensitive (Fig. 6). These results suggested that the transport mechanism of *hRFT2* differs from those of hRFT1 and hRFT3. Moreover, hRFT2 has 42.9 and 44.1% identity with hRFT1 and hRFT3, respectively, although hRFT1 and hRFT3 exhibit 86.7% identity (Supplemental Fig. 1). From the functional characterizations and sequence analyses, hRFT1 and hRFT3, but not hRFT2, have similar characteristics.

hRFT1 and hRFT2 were strongly expressed in the small intestine (Fig. 2). The characteristics of hRFT2 are similar to the carrier-mediated riboflavin uptake from the apical side of the Caco-2 human intestinal epithelial cells in terms of the affinity for riboflavin, Na^+-dependency, pH-dependency, and substrate specificity (Figs. 5*C*, 6, 7*C*; Supplemental Fig. 2*A*) (20). These data, however, contradict previous reports using small intestinal tissue specimens and brush border membrane vesicles from the perspective of Na^+-dependency (21–26). On the other hand, the uptake of riboflavin by the basolateral membrane vesicles isolated from the small intestine was independent of Na^+ and pH (27); therefore, the features of hRFT1 resemble those of the basolateral membrane (Fig. 6; Supplemental Fig. 2*A*). Although further studies about the membrane localization and the driving force of hRFT1 and hRFT2 are needed, the present findings suggest that 2 different types riboflavin transporters, hRFT1 and hRFT2, play cooperative roles in riboflavin transport in the small intestine.

Riboflavin consists of an isoalloxazine ring and ribose side chain and is converted to 2 coenzyme forms, FMN and FAD, in the cell. FMN has a phosphate group attached to the α carbon of the ribityl side chain, and FAD has ADP attached at the ribose moiety. Its photolytic degradation product, lumiflavine, has a methyl group substituting for the ribose side chain. The chemical structures of these analogs are shown in Figure 7*A*. The transport activity of hRFT was completely inhibited by lumiflavine, but not D-ribose (Fig. 7*B–D*), suggesting that the isoalloxazine ring of riboflavin, but not the ribose side chain, is necessary for recognition of all hRFT. In addition, the inhibitory effect of FMN on riboflavin transport was stronger than that of FAD, but weaker than that of unlabeled riboflavin. Therefore, the addition of phosphate and ADP to riboflavin could disturb its binding to all hRFT. The substrate specificities of hRFT were similar and relatively specific for riboflavin, as shown in this study and previously reported (Fig. 7) (3,8). hRFT might specifically recognize the isoalloxazine ring of riboflavin as the substrate.

In conclusion, we isolated a new human riboflavin transporter, hRFT3, which could play an important role in riboflavin homeostasis of the brain. hRFT3 is similar to hRFT1, but not to *hRFT2*, in amino acid sequence homology and functional characteristics. The present study provides important information about the involvement of hRFT in the homeostasis of riboflavin.

Acknowledgments

A.Y., S.M., and T.K. designed the research; Y.Y., A.Y., and H.Y. conducted the research and analyzed the data; Y.Y., A.Y., and H.Y. wrote the paper; S.M., T.K., and K.I. provided critical review of the paper; and K.I. had primary responsibility for final content. All authors read and approved the final manuscript.

Literature Cited

1. Powers HJ. Riboflavin (vitamin B-2) and health. Am J Clin Nutr. 2003;77:1352–60.
2. Foraker AB, Khantwal CM, Swaan PW. Current perspectives on the cellular uptake and trafficking of riboflavin. Adv Drug Deliv Rev. 2003;55:1467–83.
3. Yonezawa A, Masuda S, Katsura T, Inui K. Identification and functional characterization of a novel human and rat riboflavin transporter, RFT1. Am J Physiol Cell Physiol. 2008;295:C632–41.
4. Hirokawa T, Boon-Chieng S, Mitaku S. SOSUI: classification and secondary structure prediction system for membrane proteins. Bioinformatics. 1998;14:378–9.
5. Burgess CM, Slotboom DJ, Geertsma ER, Duurkens RH, Poolman B, van Sinderen D. The riboflavin transporter RibU in Lactococcus lactis: molecular characterization of gene expression and the transport mechanism. J Bacteriol. 2006;188:2752–60.
6. Vitreschak AG, Rodionov DA, Mironov AA, Gelfand MS. Regulation of riboflavin biosynthesis and transport genes in bacteria by transcriptional and translational attenuation. Nucleic Acids Res. 2002;30:3141–51.
7. Reihl P, Stolz J. The monocarboxylate transporter homolog Mch5p catalyzes riboflavin (vitamin B2) uptake in Saccharomyces cerevisiae. J Biol Chem. 2005;280:39809–17.
8. Yamamoto S, Inoue K, Ohta K, Fukatsu R, Maeda J, Yoshida Y, Yuasa H. Identification and functional characterization of rat riboflavin transporter 2. J Biochem. 2009;145:437–43.
9. Motohashi H, Sakurai Y, Saito H, Masuda S, Urakami Y, Goto M, Fukatsu A, Ogawa O, Inui K. Gene expression levels and immunolocalization of organic ion transporters in the human kidney. J Am Soc Nephrol. 2002;13:866–74.
10. Urakami Y, Akazawa M, Saito H, Okuda M, Inui K. cDNA cloning, functional characterization, and tissue distribution of an alternatively spliced variant of organic cation transporter hOCT2 predominantly expressed in the human kidney. J Am Soc Nephrol. 2002;13:1703–10.
11. Farrell CL, Pardridge WM. Blood-brain barrier glucose transporter is asymmetrically distributed on brain capillary endothelial lumenal and ablumenal membranes: an electron microscopic immunogold study. Proc Natl Acad Sci USA. 1991;88:5779–83.
12. Thorens B, Sarkar HK, Kaback HR, Lodish HF. Cloning and functional expression in bacteria of a novel glucose transporter present in liver, intestine, kidney, and beta-pancreatic islet cells. Cell. 1988;55:281–90.
13. Fukumoto H, Seino S, Imura H, Seino Y, Eddy RL, Fukushima Y, Byers MG, Shows TB, Bell GI. Sequence, tissue distribution, and chromosomal localization of mRNA encoding a human glucose transporter-like protein. Proc Natl Acad Sci USA. 1988;85:5434–8.
14. Sotiriou S, Gispert S, Cheng J, Wang Y, Chen A, Hoogstraten-Miller S, Miller GF, Kwon O, Levine M, et al. Ascorbic-acid transporter Slc23a1 is essential for vitamin C transport into the brain and for perinatal survival. Nat Med. 2002;8:514–7.
15. Tsukaguchi H, Tokui T, Mackenzie B, Berger UV, Chen XZ, Wang Y, Brubaker RF, Hediger MA. A family of mammalian Na^+-dependent L-ascorbic acid transporters. Nature. 1999;399:70–5.
16. Nagatsu T, Nagatsu-Ishibashi I, Okuda J, Yagi K. Incorporation of peripherally administered riboflavine into flavine nucleotides in the brain. J Neurochem. 1967;14:207–10.
17. Spector R, Boose B. Active transport of riboflavin by the isolated choroid plexus in vitro. J Biol Chem. 1979;254:10286–9.
18. Burch HB, Combs AM, Lowry OH, Padilla AM. Effects of riboflavin deficiency and realimentation on flavin enzymes of tissues. J Biol Chem. 1956;223:29–45.
19. Spector R. Riboflavin accumulation by rabbit brain slices in vitro. J Neurochem. 1980;34:1768–71.

20. Said HM, Ma TY. Mechanism of riboflavine uptake by Caco-2 human intestinal epithelial cells. Am J Physiol Gastrointest Liver Physiol. 1994;266:G15–21.
21. Hegazy E, Schwenk M. Riboflavin uptake by isolated enterocytes of guinea pigs. J Nutr. 1983;113:1702–7.
22. Said HM, Arianas P. Transport of riboflavin in human intestinal brush border membrane vesicles. Gastroenterology. 1991;100:82–8.
23. Daniel H, Rehner GI. Sodium-dependent transport of riboflavin in brush border membrane vesicles of rat small intestine is an electrogenic process. J Nutr. 1992;122:1454–61.
24. Tomei S, Yuasa H, Inoue K, Watanabe J. Transport functions of riboflavin carriers in the rat small intestine and colon: site difference and effects of tricyclic-type drugs. Drug Deliv. 2001;8:119–24.
25. Middleton HM. Uptake of riboflavin by rat intestinal mucosa in vitro. J Nutr. 1990;120:588–93.
26. Daniel H, Wille U, Rehner G. In vitro kinetics of the intestinal transport of riboflavin in rats. J Nutr. 1983;113:636–43.
27. Said HM, Hollander D, Mohammadkhani R. Uptake of riboflavin by intestinal basolateral membrane vesicles: a specialized carrier-mediated process. Biochim Biophys Acta. 1993;1148:263–8.

Journal of Gastroenterology and Hepatology

JGHF

doi:10.1111/j.1440-1746.2009.06206.x

GASTROENTEROLOGY

Efficacy and safety of infliximab as rescue therapy for ulcerative colitis refractory to tacrolimus

Shuji Yamamoto,*,† Hiroshi Nakase,* Minoru Matsuura,* Yusuke Honzawa,* Satohiro Masuda,‡ Ken-ichi Inui‡ and Tsutomu Chiba*

*Department of Gastroenterology and Hepatology, Graduate School of Medicine, Kyoto University, Kyoto, †Research Fellow of the Japan Society for the Promotion of Science, Tokyo, and ‡Department of Pharmacy, Kyoto University Hospital, Kyoto, Japan

Key words
infliximab, tacrolimus, ulcerative colitis.

Accepted for publication 16 November 2009.

Correspondence
Dr Hiroshi Nakase, Department of Gastroenterology and Hepatology, Graduate School of Medicine, Kyoto University, 54 Shogoin Kawahara-cho, Sakyo-ku, Kyoto 606-8507, Japan. Email: hiropy_n@kuhp.kyoto-u.ac.jp

Abstract

Background and Aim: Little is known about the efficacy and safety of infliximab for ulcerative colitis refractory to tacrolimus. The aim of this study was to evaluate the efficacy and safety of infliximab in the induction of remission in ulcerative colitis patients with persistent symptoms despite tacrolimus therapy.

Methods: We report a retrospective, observational, single-center case series of 12 consecutively enrolled patients with ulcerative colitis refractory to tacrolimus that received infliximab therapy for the induction of remission. Eight patients received a single infusion of infliximab, and four received two or more infusions. Median follow-up duration was 16.0 months (range, 1.6–41.4 months). The clinical response was evaluated based on a modified Truelove-Witts severity index.

Results: Six patients (50.0%) achieved clinical remission within 30 days. Overall cumulative colectomy-free survival was estimated to be 58.3% at 41.4 months. Adverse events included an elevation of liver enzymes (1/12; 8.3%) and a mild infusion reaction (1/12; 8.3%). No mortality occurred.

Conclusions: Infliximab can induce remission in patients with ulcerative colitis who do not tolerate or respond to tacrolimus therapy.

Introduction

Ulcerative colitis (UC) is an idiopathic, chronic, and inflammatory disorder characterized by diarrhea, rectal bleeding, abdominal pain, fever, anemia, and body weight loss.[1] Corticosteroid therapy is used for patients with UC who do not respond to aminosalicylates or those with a severe attack of UC.[1–3] Although most patients with UC initially respond to corticosteroids, approximately 20% of patients with UC become steroid-dependent and 30% of those require surgery within 1 year after initiating corticosteroid therapy.[4]

Tacrolimus is reported to be effective for patients with ulcerative colitis (UC) refractory to steroids. One placebo-controlled study[1] and several uncontrolled studies[6–10] demonstrated the short-term efficacy of tacrolimus treatment in patients with UC, and there are several reports on the long-term effects.[6–8] Recently, we demonstrated both the short- and long-term efficacy of tacrolimus for refractory UC.[11] In that study, 21 of 27 (77.8%) patients had a clinical response and overall cumulative colectomy-free survival was 62.3% at 65 months.[11] Some patients with refractory UC, however, do not have a clinical response to tacrolimus or relapse even after clinical remission with tacrolimus therapy is achieved.

Infliximab (IFX) is a chimeric IgG1 monoclonal antibody to tumor necrosis factor-alpha (TNFα) that binds with high affinity to TNFα, neutralizing its biologic activity.[12] The Active Ulcerative Colitis Trials (ACT) 1 and 2 proved the efficacy of IFX in inducing and maintaining a clinical response and remission in patients with moderate or severe UC.[13] In patients who received IFX, 61% to 69% had a clinical response at week 8, while 29% to 37% of those who received placebo had a clinical response in these studies. In ACT 1, a clinical response was achieved at week 54 in significantly more patients who received IFX than those who received placebo.

Patients with steroid-refractory UC who failed second-line therapies with cyclosporine, tacrolimus, or IFX have limited medical options to achieve remission and avoid colectomy. Recently, the effect of IFX as rescue therapy on patients with steroid-refractory UC who did not respond to cyclosporine was reported by two groups. Maser *et al.*[14] demonstrated that four (40%) of 10 patients achieved remission, two (20%) responded to IFX therapy, and six (60%) avoided colectomy or death during an average follow-up period of 7.8 months. Mañosa *et al.*[15] reported that 10 (62.5%) of 16 patients avoided colectomy during median follow-up from the first IFX infusion of 195 days.

Table 1 Modified Truelove Witts severity index (MTWSI)[16]

Score	0	1	2	3	4	5
Bowel movement	0–2	3–4	5–6	7–9	≥ 10	
Nocturnal diarrhea	No	Yes				
Visible blood in stool	0%	< 50%	≥ 50%	100%		
Abdominal tenderness	None	Mild	Moderate	Severe		
Abdominal pain/cramping	None	Mild	Moderate	Severe		
Need for antidiarrheals	No	Yes				
General status	Perfect	Very good	Good	Average	Poor	Terrible
Fecal incontinence	No	Yes				

Severe category: 10 or higher; remission category: 4 or less.

To our knowledge, however, there are no reports on the effect of IFX as rescue therapy for patients with UC refractory to tacrolimus. We herein report the efficacy and safety of IFX therapy in patients with steroid-refractory UC who failed tacrolimus therapy.

Methods

Patients

Between November 2005 and October 2009, 12 patients with steroid-refractory UC who were also refractory to tacrolimus were consecutively enrolled in this retrospective, observational, single-center study, and all patients received IFX (Remicade: Centocor, Malvern, PA, USA) therapy for the induction of remission. This study was approved by the Institutional Review Board of Kyoto University. Patients were informed about the potential risks and benefits of IFX therapy and all provided informed written consent to its use. In all cases, the diagnosis was established according to standardized criteria by prior clinical assessment, radiology, endoscopy, and histology. Patients either did not respond or could not tolerate tacrolimus therapy. Rescue therapy was defined as having received IFX concomitant with tacrolimus or within 4 weeks of discontinuing tacrolimus.

Definition of response

Disease activity was evaluated using a modified Truelove-Witts severity index (MTWSI),[16] details are shown in Table 1. The potential maximum (worst) score was 21 and the potential minimum (best) score was 0. Clinical remission was retrospectively defined as an estimated MTWSI score of 4 or less. Relapse was defined as an increase in the MTWSI score to 5 or higher with additional therapies required, including corticosteroids, thioprines, cytapheresis, and surgery in patients who had initially achieved clinical remission by IFX therapy.

Treatment

In all patients, IFX was given at a dose of 5 mg/kg body weight as a 2-h intravenous infusion. Eight patients were hospitalized during IFX infusion, and four received IFX as outpatients. Tacrolimus and other drugs including thioprines were continued unless side-effects such as impaired renal function or infectious disease were observed. Tacrolimus whole-blood trough concentrations were monitored and aimed to be maintained between 5 and 10 ng/mL. The disease course was evaluated clinically with routine laboratory tests, and patients were regularly interviewed about adverse events on each visit.

Assessment and statistics

The primary endpoints of this study were the induction of remission and colectomy-free survival. The secondary endpoint was treatment safety.

Proportions between two groups were compared by Fisher's exact test and continuous variables were compared by Mann–Whitney *U*-test. Clinical scores in clinical courses were compared by Wilcoxon signed-rank test. Colectomy-free survival was assessed using the Kaplan–Meier method. A *P*-value of less than 0.05 was considered to be statistically significant.

Results

Patient characteristics

Patient characteristics at baseline are shown in Table 2. Of the 12 patients treated with IFX, four were male (33.3%) and eight were female (66.7%), with a median age at IFX infusion of 57 years (range, 18–69 years). The median disease duration prior to IFX treatment was 56 months (range, 7–351 months). Six patients (50.0%) had severe disease with the MTWSI score of 10 or more at the start of treatment and the remaining six (50.0%) had moderate disease with the MTWSI score of 7–9. Nine of the patients (75.0%) had pancolitis and three (25.0%) had left-sided colitis. None of the patients had proctitis. Of 12 patients, 10 patients (83.4%) had steroid dependency, which was defined as either chronic active UC for more than 6 months or more than once a year, or at least three times every 2 years regardless of intensive medical therapy, including corticosteroids.[5] One patient (8.3%) was steroid-resistant, which was defined as having a lack of response to a systemic daily dose of 30 mg or more of prednisone per body over at least 2 weeks.[5] One patient (8.3%) was steroid-naive. The total amount of administered corticosteroids prior to IFX therapy in each patient was not available because most of the enrolled patients were referred to our hospital from other hospitals without data on this issue. Although 11 of 12 patients had a history of steroid therapy, only one patient (8.3%) received corticosteroids at the time of IFX infusion because corticosteroids could be withdrawn with tacrolimus in the other 10 patients. Thioprines were given concomitant with tacrolimus in three patients (25.0%). Two

Table 2 Patient baseline characteristics

Patient	Age and sex	Disease site	Disease duration at IFX infusion	MTWSI at IFX infusion	Response to corticosteroids	Dose of predonisolone at IFX infusion
1	47 F	Pancolitis	54 months	7	Dependent	N.A.
2	64 M	Pancolitis	105 months	14	Dependent	N.A.
3	64 M	Pancolitis	45 months	7	Dependent	N.A.
4	34 F	Pancolitis	7 months	11	Dependent	N.A.
5	69 F	Pancolitis	19 months	9	Dependent	N.A.
6	20 F	Pancolitis	73 months	8	Dependent	5 mg/day
7	18 F	Pancolitis	32 months	10	Dependent	N.A.
8	60 F	Pancolitis	56 months	12	Dependent	N.A.
9	67 F	Left-sided	274 months	8	Dependent	N.A.
10	54 M	Left-sided	351 months	7	Dependent	N.A.
11	36 M	Left-sided	56 months	10	Resistant	N.A.
12	61 F	Pancolitis	349 months	12	Naive	N.A.

F, female; IFX, infliximab; M, male; MTWSI, modified Truelove-Witts severity index; N.A., not administered.

Table 3 Infusion of infliximab (IFX) therapy, cytomegalovirus reactivation during infliximab treatment, and outcome of treatment

Patient	No. IFX infusions for induction of remission	CMV reactivation during IFX treatment	Response to IFX	Final outcome (end of follow up)	Duration of follow up
1	1	No	Remission	Chronic active; FK, 6MP	41.4 months
2	2	Yes	Not respond	Colectomy	1.6 months
3	1	No	Not respond	Remission; 5ASA	37.8 months
4	1	Yes	Remission	Colectomy	5.0 months
5	1	No	Not respond	Colectomy	4.4 months
6	1	No	Not respond	Chronic active; FK, PSL	34.5 months
7	1	No	Remission	Remission; 6MP	34.3 months
8	1	Yes	Not respond	Colectomy	5.7 months
9	1	Yes	Remission	Remission; IFX	23.0 months
10	3	No	Remission	Remission; IFX, FK, AZA	17.0 months
11	3	No	Remission	Remission; IFX, 6MP	14.9 months
12	3	Yes	Not respond	Colectomy	3.1 months

5ASA, 5-aminosalitirate; 6MP, 6-mercaptopurine; AZA, azathioprine; CMV, cytomegalovirus; FK, tacrolimus; PSL, predonisolone.

(16.7%) of 12 patients had been treated with cytapheresis. All patients had been treated with either 5-aminosalicylic acid or salazosulfapyridine. Six patients (50.0%) had no clinical response to tacrolimus and four (33.3%) relapsed during tacrolimus therapy for maintaining remission. Two patients (16.7%) terminated tacrolimus therapy before IFX administration. One patient discontinued tacrolimus due to gingival infection and relapsed 2 weeks after tacrolimus discontinuation, while the other patient stopped tacrolimus because of reactivation of cytomegalovirus during flare up of UC.

Induction of remission

Of the 12 patients, eight (66.7%) received a single infusion of IFX and four (33.3%) received two or three infusions (Table 3). Immediate outcome was assessed 15 days and 30 days after the first infusion of IFX, based on the MTWSI score. Six (50.0%) of 12 patients achieved clinical remission within 30 days after IFX infusion (Table 3). None of the patients underwent colectomy in the 30 days after the first infusion of IFX. Median MTWSI score decreased from 9.5 at the time of the first IFX infusion to 5.5 at 15 days and 5 at 30 days after the start of the treatment (Fig. 1). MTWSI score at both 15 and 30 days was significantly lower than that before IFX infusion (Wilcoxon signed rank test; $P < 0.01$). Patient characteristics did not differ significantly between those who responded to IFX therapy and those who did not (Table 4).

Colectomy-free survival

Patients were followed for a median of 16.0 months (range, 1.6–41.4 months) after the initiation of IFX therapy. Within a median follow-up of 16.0 months, five patients (41.7%) underwent colectomy between 1.6 and 5.7 months following the first infusion of IFX (Table 3). Eleven patients were free from corticosteroids. Based on Kaplan–Meier survival analysis, the overall cumulative colectomy-free survival was estimated to be 58.3% at 41.4 months (Fig. 2). Clinical characteristics of patients who underwent colectomy and of those who avoided colectomy are summarized in Table 5. In patients who avoided colectomy, the MTWSI score at the time of the first infusion of IFX was significantly lower than that in the five patients who underwent colectomy. With the exception of the MTWST score, no other patient characteristics were significantly associated with colectomy.

Adverse effects

None of the patients reported severe adverse events and all adverse events were controlled by conservative therapy. Only one patient (8.3%) experienced a mild infusion reaction, and there were no severe infusion reactions that required discontinuation of treatment. One patient (8.3%) experienced a mild elevation of liver enzymes. No mortality occurred during this treatment.

Discussion

The management of patients with steroid-refractory UC who fail second-line therapies, including cyclosporine, tacrolimus, and IFX, remains challenging. Most of these patients eventually undergo colectomy, but the quality of life is not always satisfactory for these patients compared with those who respond to medical therapy.[17] Therefore, establishing rescue therapies for patients with steroid-refractory UC who do not respond to IFX or calcineurin inhibitors, including cyclosporine and tacrolimus, is very impor-

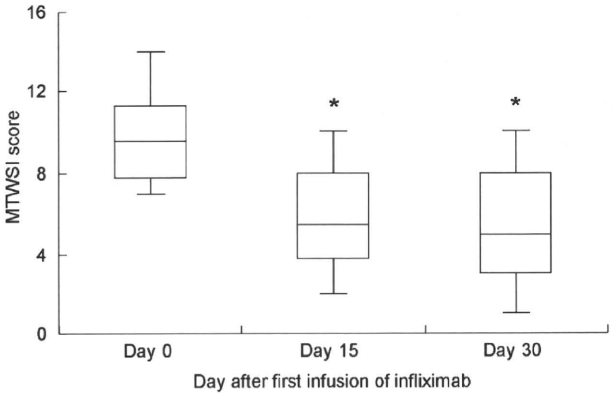

Figure 1 Changes in Modified Truelove Witts severity index (MTWSI) scores during infliximab (IFX) treatment ($n = 12$). The MTWSI decreased significantly at 15 days and 30 days after the initiation of IFX treatment (Wilcoxon signed rank test). The interquartile range (IQR) is represented by the box, with the median MTWSI value indicated by the line within the box. *P-value < 0.01.

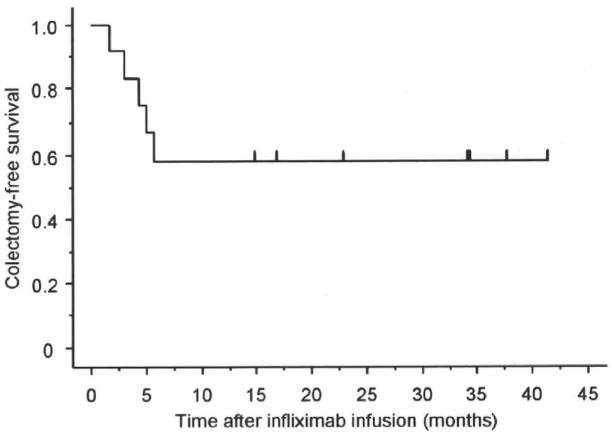

Figure 2 Proportion of patients that avoided colectomy ($n = 12$). The overall cumulative colectomy-free survival was estimated to be 58.3% at 41.4 months, based on Kaplan–Meier survival analysis.

Table 4 Clinical characteristics of patients who responded to infliximab (IFX) and those who did not

Variable	Responders ($n = 6$)	Non-responders ($n = 6$)	P-value
Age at onset of the disease (years, median)	32.5	52	0.1720
Age at first IFX infusion (years, median)	41.5	62.5	0.1488
Sex (male/female)	2/4	2/4	1.0000
Disease type (pancolitis/left-sided colitis)	3/3	6/0	0.1818
Disease duration at first IFX infusion (months, median)	55	89	0.4704
MTWSI score at first IFX infusion (median)	9	10.5	0.2920
IFX infusion (single infusion/two or more infusions)	4/2	4/2	1.0000

MTWSI, modified Truelove-Witts severity index.

Table 5 Clinical characteristics of patients who underwent colectomy and those who avoided colectomy

Variable	Not-colectomized patients ($n = 7$)	Colectomy patients ($n = 5$)	P-value
Age at onset of the disease (years, median)	31	49	0.1923
Age at first IFX infusion (years, median)	47	61	0.2548
Sex (male/female)	3/4	1/4	0.5758
Disease type (pancolitis/left-sided colitis)	4/3	5/0	0.2045
Disease duration at first IFX infusion (months, median)	56	105	0.7449
MTWSI score at first IFX infusion (median)	**8**	**12**	**0.0108**
IFX infusion (single infusion/two or more infusions)	5/2	3/2	1.0000

IFX, infliximab; MTWSI, modified Truelove-Witts severity index.

tant. To our knowledge, the present case series is the first to demonstrate the effects and safety of IFX in patients with UC refractory to tacrolimus.

First, we evaluated the effects of IFX therapy in the induction of remission. Of 12 patients who did not achieve remission with tacrolimus or relapsed despite tacrolimus therapy, six (50.0%) achieved clinical remission within 30 days after the first IFX infusion. IFX therapy is reported to be effective for patients with steroid-refractory UC who did not respond to cyclosporine as a second-line of medical therapy.[14] In that study, four (40%) of 10 patients achieved remission and two (20%) responded to IFX therapy. These findings suggested that IFX, which has been already used as a second-line medical therapy for patients with steroid-refractory UC, could be useful as a third-line medical therapy for patients with steroid-refractory UC who did not respond to calcineurin inhibitors.

One of the most important clinical outcomes in refractory UC is colectomy-free survival rate over the medium- to long-term after IFX induction therapy. There are several reports on the long-term efficacy of IFX therapy for patients with UC refractory to corticosteroids, demonstrating a survival rate free from colectomy of 53% to 89% during a median follow-up period of approximately 1–3 years.[18–20] One study[14] reported that of 10 patients with UC refractory to cyclosporine that received IFX, six (60%) avoided colectomy or death during an average follow-up period of 7.8 months. The other study[15] demonstrated that 10 (62.5%) of 16 patients avoided colectomy during median follow up from the first IFX infusion of 195 days.

Similarly, in our series, seven (58.3%) of 12 patients avoided colectomy during a median follow-up period of 16.0 months. These findings suggested that most of the patients who responded to third-line medical therapy using IFX for steroid-refractory UC might avoid surgery over the medium-term, or for approximately 1 year.

Univariate analysis in our study showed that a higher MTWSI score at the time of the initiation of IFX therapy was significantly associated with eventual colectomy (Table 4). Some studies investigated predictive factors for colectomy in IFX therapy as second-line medical therapy in steroid-refractory UC. Kohn *et al.*[18] reported that early colectomy rates were higher in patients receiving one infusion compared with those receiving two or more infusions. Jakobovits *et al.*[20] demonstrated that patients diagnosed with UC at a younger age were at higher risk for colectomy. In these studies, however, there was no significant association between disease activity at the time of the first infusion and colectomy. Jarnerot *et al.*[21] reported a significant reduction in the 30-day colectomy rate in a cohort with moderate to severe UC (characterized by the Seo index), but no significant difference in the cohort with more severe UC (characterized by the Sweden Index), similar to our series. In this regard, further evaluation is required to elucidate predictive factors for the outcome of IFX therapy.

An important question in the treatment of patients with corticosteroid-refractory UC is whether IFX should be given initially or after failing to respond to therapies using calcineurin inhibitors, including cyclosporine and tacrolimus. Our case series did not include UC patients who received tacrolimus after failure of IFX treatment. Maser *et al.*[14] demonstrated a similar remission induction rate and colectomy-free survival in IFX therapy for cyclosporine-refractory UC and cyclosporine therapy for IFX-refractory UC. It may be reasonable that calcineurin inhibitors should be given initially as Maser *et al.* stated,[14] because an elimination half-life of these agents (tacrolimus: 12 h,[22] cyclosporine: 6 h[23]) is much shorter than that of IFX (18.5 days[24]). To elucidate this clinical issue, however, a clinical randomized controlled trial on the outcome of IFX administration after failure of calcineurin inhibitors, and vice versa, is necessary.

Because the immunosuppressive mechanism of tacrolimus differs from that of IFX, concomitant use of these drugs might increase the risk of opportunistic infections. In the case series on third-line medical therapy for steroid refractory UC, one patient died of Gram-negative sepsis at 2 weeks after the initiation of third-line therapy using IFX in the report by Maser *et al.*,[14] and one severe infectious complication was noticed in that by Mañosa *et al.*[15] Of note, infectious disease was not observed in our series, although the number of enrolled patients was small. The immunosuppressive effect of tacrolimus is 30–100 times greater *in vitro* and 10–20 times greater *in vivo* than that of cyclosporine,[25] and remission rate by tacrolimus therapy in UC in our hospital was 77.8%,[11] which is comparable to that by cyclosporine reported previously.[26,27] Recent studies demonstrated that the use of corticosteroids is associated with serious infections in patients with inflammatory bowel disease,[28–30] and in our series, only one patient received concomitant corticosteroid administration. Considering these facts, the reason why adverse effects in our patients were smaller compared with those in patients who received IFX after cyclosporine[14,15] may be that fewer numbers of patients have used corticosteroids during IFX therapy. Therefore, tapering corticosteroids might be necessary to avoid serious infectious disease during third-line medical therapy for refractory UC.

There are some limitations to our study, including a small sample size and therapeutic protocol. Although our sample size was small, the efficacy of IFX therapy as a third-line therapy was promising. Clinical trials with a large number of patients with refractory UC are required to confirm these preliminary results. In the present study, a single infusion of IFX was performed as an induction therapy in most enrolled patients. In the ACT 1 and 2 trials,[13] three infusions of IFX at 0, 2, and 8 weeks were performed for an induction regimen.[31,32] The favorable effect of a single infusion of IFX on patients with refractory UC, however, has been reported.[21,33,34] In addition, to date there have been no controlled studies comparing the therapeutic effect of a single infusion of IFX with that of three infusions in UC patients. Further evaluation is required to optimize the induction regimen for IFX therapy.

In conclusion, the administration of IFX in patients with corticosteroid-refractory UC who did not respond to tacrolimus is effective and well-tolerated. Further studies are required to elucidate whether calcineurin inhibitors or IFX should be given first in patients with corticosteroid-refractory UC.

Acknowledgments

This work was supported by a Grant-in-Aid for Scientific Research (C) from the Ministry of Culture and Science of Japan (grant 18590677), the Kato Memorial Trust for Nambyo Research, Japan Foundation for Applied Enzymology and the Shimizu Foundation for the Promotion of Immunology Research (to HN); and by Grants-in-Aid for Scientific Research (16017240, 16017249, 17013051, 17659212, and 18012029) from the Ministry of

Education, Culture, Sports, Science, and Technology of Japan, Grants-in-Aid for Scientific Research (15209024 and 18209027) from JSPS, and a Grant-in-Aid for Research on Measures for Intractable Disease, and Research on Advanced Medical Technology (nano005) from the Ministry of Health, Labor, and Welfare, Japan (to TC).

References

1 Podolsky DK. Inflammatory bowel disease. *N. Engl. J. Med.* 2002; **347**: 417–29.
2 Sands BE. Inflammatory bowel disease: past, present, and future. *J. Gastroenterol.* 2007; **42**: 16–25.
3 Baumgart DC, Sandborn WJ. Inflammatory bowel disease: clinical aspects and established and evolving therapies. *Lancet* 2007; **369**: 1641–157.
4 Faubion WA Jr, Loftus EV Jr, Harmsen WS, Zinsmeister AR, Sandborn WJ. The natural history of corticosteroid therapy for inflammatory bowel disease: a population-based study. *Gastroenterology* 2001; **121**: 255–60.
5 Ogata H, Matsui T, Nakamura M *et al.* A randomized dose finding study of oral tacrolimus (FK506) therapy in refractory ulcerative colitis A randomized dose finding study of oral tacrolimus. *Gut* 2006; **55**: 1255–62.
6 Baumgart DC, Pintoffl JP, Sturm A, Wiedenmann B, Dignass AU. Tacrolimus is safe and effective in patients with severe steroid-refractory or steroid-dependent inflammatory bowel disease—a long-term follow-up. *Am. J. Gastroenterol.* 2006; **101**: 1048–56.
7 Fellermann K, Tanko Z, Herrlinger KR *et al.* Response of refractory colitis to intravenous or oral tacrolimus (FK506). *Inflamm. Bowel. Dis.* 2002; **8**: 317–24.
8 Ng SC, Arebi N, Kamm MA. Medium-term results of oral tacrolimus treatment in refractory inflammatory bowel disease. *Inflamm. Bowel. Dis.* 2007; **13**: 129–34.
9 Ziring DA, Wu SS, Mow WS, Martín MG, Mehra M, Ament ME. Oral tacrolimus for steroid-dependent and steroid-resistant ulcerative colitis in children. *J. Pediatr. Gastroenterol. Nutr.* 2007; **45**: 306–11.
10 Högenauer C, Wenzl HH, Hinterleitner TA, Petritsch W. Effect of oral tacrolimus (FK 506) on steroid-refractory moderate/severe ulcerative colitis. *Aliment. Pharmacol. Ther.* 2003; **18**: 415–23.
11 Yamamoto S, Nakase H, Mikami S *et al.* Long-term effect of tacrolimus therapy in patients with refractory ulcerative colitis. *Aliment. Pharmacol. Ther.* 2008; **28**: 589–97.
12 Knight DM, Trinh H, Le J *et al.* Construction and initial characterization of a mouse-human chimeric anti-TNF antibody. *Mol. Immunol.* 1993; **30**: 1443–53.
13 Rutgeerts P, Sandborn WJ, Feagan BG *et al.* Infliximab for induction and maintenance therapy for ulcerative colitis. *N. Engl. J. Med.* 2005; **353**: 2462–76.
14 Maser EA, Deconda D, Lichtiger S, Ullman T, Present DH, Kornbluth A. Cyclosporine and infliximab as rescue therapy for each other in patients with steroid-refractory ulcerative colitis. *Clin. Gastroenterol. Hepatol.* 2008; **6**: 1112–16.
15 Mañosa M, López San Román A, Garcia-Planella E *et al.* Infliximab rescue therapy after cyclosporin failure in steroid-refractory ulcerative colitis. *Digestion* 2009; **80**: 30–5.
16 Lichtiger S, Present DH. Preliminary report: cyclosporin in treatment of severe active ulcerative colitis. *Lancet* 1990; **336**: 16–19.
17 Cohen RD, Brodsky AL, Hannauer SB. A comparison of the quality of life in patients with severe ulcerative colitis after total colectomy versus medical treatment with intravenous cyclosporin. *Inflamm. Bowel. Dis.* 1999; **5**: 1–10.
18 Kohn A, Daperno M, Armuzzi A *et al.* Infliximab in severe ulcerative colitis: short-term results of different infusion regimens and long-term follow-up. *Aliment. Pharmacol. Ther.* 2007; **26**: 747–56.
19 Ferrante M, Vermeire S, Katsanos KH *et al.* Predictors of early response to infliximab in patients with ulcerative colitis. *Inflamm. Bowel. Dis.* 2007; **13**: 123–8.
20 Jakobovits SL, Jewell DP, Travis SP. Infliximab for the treatment of ulcerative colitis: outcomes in Oxford from 2000–2006. *Aliment. Pharmacol. Ther.* 2007; **25**: 1055–60.
21 Järnerot G, Hertervig E, Friis-Liby I *et al.* Infliximab as rescue therapy in severe to moderately severe ulcerative colitis: a randomized, placebo-controlled study. *Gastroenterology* 2005; **128**: 1805–11.
22 Venkataramanan R, Swaminathan A, Prasad T *et al.* Clinical pharmacokinetics of tacrolimus. *Clin. Pharmacokinet.* 1995; **29**: 404–30.
23 Ptachcinski RJ, Venkataramanan R, Burckart GJ *et al.* Cyclosporine kinetics in healthy volunteers. *J. Clin. Pharmacol.* 1987; **27**: 243–8.
24 Ternant D, Aubourg A, Magdelaine-Beuzelin C *et al.* Infliximab pharmacokinetics in inflammatory bowel disease patients. *Ther. Drug. Monit.* 2008; **30**: 523–9.
25 Kino T, Hatanaka H, Miyata S *et al.* FK-506, a novel immunosuppressant isolated from a Streptomyces. II. Immunosuppressive effect of FK-506 *in vitro*. *J. Antibiot. (Tokyo)* 1987; **40**: 1256–65.
26 Lichtiger S, Present DH, Kornbluth A *et al.* Cyclosporine in severe ulcerative colitis refractory to steroid therapy. *N. Engl. J. Med.* 1994; **330**: 1841–5.
27 Carbonnel F, Boruchowicz A, Duclos B *et al.* Intravenous cyclosporine in attacks of ulcerative colitis: short term and long term responses. *Dig. Dis. Sci.* 1996; **41**: 2471–6.
28 Lichtenstein GR, Feagan BG, Cohen RD *et al.* Serious infections and mortality in association with therapies for Crohn's disease: TREAT registry. *Clin. Gastroenterol. Hepatol.* 2006; **4**: 621–30.
29 Fidder H, Schnitzler F, Ferrante M *et al.* Long-term safety of infliximab for the treatment of inflammatory bowel disease: a single-centre cohort study. *Gut* 2009; **58**: 501–8.
30 Ferrante M, D'Hoore A, Vermeire S *et al.* Corticosteroids but not infliximab increase short-term postoperative infectious complications in patients with ulcerative colitis. *Inflamm. Bowel. Dis.* 2009; **15**: 1062–70.
31 Hanauer SB, Feagan BG, Lichtenstein GR *et al.* Maintenance infliximab for Crohn's disease: the ACCENT I randomised trial. *Lancet* 2002; **359**: 1541–9.
32 Sands BE, Anderson FH, Bernstein CN *et al.* Infliximab maintenance therapy for fistulizing Crohn's disease. *N. Engl. J. Med.* 2004; **350**: 876–85.
33 Su C, Salzberg BA, Lewis JD *et al.* Efficacy of anti-tumor necrosis factor therapy in patients with ulcerative colitis. *Am. J. Gastroenterol.* 2002; **97**: 2577–84.
34 Gornet JM, Couve S, Hassani Z *et al.* Infliximab for refractory ulcerative colitis or indeterminate colitis: an open label multicentre study. *Aliment. Pharmacol. Ther.* 2003; **18**: 175–81.

Am J Physiol Renal Physiol 298: F923–F934, 2010.
First published January 13, 2010; doi:10.1152/ajprenal.00567.2009.

Impact of Cyclin B2 and Cell division cycle 2 on tubular hyperplasia in progressive chronic renal failure rats

Kumiko Nishihara,[1] Satohiro Masuda,[1] Shunsaku Nakagawa,[1] Atsushi Yonezawa,[1] Takaharu Ichimura,[2] Joseph V. Bonventre,[2] and Ken-ichi Inui[1]

[1]*Department of Pharmacy, Kyoto University Hospital, Faculty of Medicine, Kyoto, Japan; and* [2]*Renal Division, Brigham and Women's Hospital, Harvard Medical School, Harvard Institutes of Medicine, Boston, Massachusetts*

Submitted 3 October 2009; accepted in final form 10 January 2010

Nishihara K, Masuda S, Nakagawa S, Yonezawa A, Ichimura T, Bonventre JV, Inui K. Impact of Cyclin B2 and Cell division cycle 2 on tubular hyperplasia in progressive chronic renal failure rats. *Am J Physiol Renal Physiol* 298: F923–F934, 2010. First published January 13, 2010; doi:10.1152/ajprenal.00567.2009.—To clarify the specific molecular events of progressive tubular damage in chronic renal failure (CRF), we conducted microarray analyses using isolated proximal tubules from subtotally nephrectomized (Nx) rats as a model of CRF. Our results clearly demonstrated time-dependent changes in gene expression profiles localized to proximal tubules. The expression of mitosis-specific genes Cyclin B2 and Cell division cycle 2 (Cdc2) was significantly and selectively increased in the proximal tubules during the compensated period but decreased to basal level in the end-stage period. Administration of everolimus, a potent inhibitor of mammalian target of rapamycin, markedly reduced compensatory hypertrophy and hyperplasia of epithelial cells, which was accompanied by complete abolishment of the expression of Cyclin B2 and Cdc2 enhancement; renal function was then severely decreased. Treatment with the Cdc2 inhibitor 2-cyanoethyl alsterpaullone clearly decreased epithelial cell hyperplasia, based on staining of phosphorylated histone H3 and Ki-67, while hypertrophy was not inhibited. In conclusion, we have demonstrated roles of Cyclin B2 and Cdc2 in the epithelial hyperplasia in response to Nx. These results advance the knowledge of the contribution of cell cycle regulators, especially M phase, in pathophysiology of tubular restoration and/or degeneration, and these two molecules are suggested to be a marker for the proliferation of proximal tubular cells in CRF.

proximal tubule; microarray; cell cycle; G_2-M; hypertrophy

IN ADDITION to glomerular filtration, renal tubular cells are important for the reabsorption and secretion of various compounds to maintain the homeostasis of body fluid. In chronic renal failure (CRF), loss of nephron mass results in compensating responses with respect to the function and structure of the kidney for minimizing the reduction in the total glomerular filtration rate (GFR); the hyperreactivity of the residual nephron results in irreversible glomerular sclerosis, tubular atrophy, and subsequent tubulointerstitial fibrosis (11, 15, 35). Previous studies have demonstrated that the decline in GFR is not associated with a decline in tubular function (13) and that the renal epithelium is intrinsically susceptible to injury because it concentrates many toxins (1). These findings suggest the importance of understanding the pathogenesis of dysfunction of tubular cells in CRF.

The subtotally nephrectomized (Nx) rat is a well-established model for understanding the pathological changes in CRF (15). With the use of this model, the effects on proximal tubular functions were examined. Several studies, including ours, have previously demonstrated the expressional and functional changes of membrane transporters in the compensated remnant kidneys and the effect of transporter levels on renal handling of ionic drugs in progressive CRF (14, 17, 20, 29, 30, 38). However, these changes were studied from a phenomenological perspective, and therefore there is only limited information on the basic molecular mechanisms and/or networks involved in the progression of tubular damage in CRF. Some candidate genes responsible for progressive renal injury were identified by microarray analysis using whole kidney samples; however, reproducibility of this strategy has been poor (40, 44).

To overcome these problems and find the responsible genes affecting tubular pathological changes in compensative CRF, we conducted a microarray analysis with isolated proximal tubules at several time points after Nx and found the expression of the mitosis-specific genes Cyclin B2 and Cell division cycle 2 (Cdc2), which are M-phase regulators, to be transiently upregulated in the proximal tubules of the compensatory kidney. Although cell cycle regulation has been demonstrated to play important roles in renal pathophysiology, these reports mainly focused on the molecules that played roles in G_1-S phase among the four stages of the cell cycle, G_1, S, G_2, and M (23, 31, 33, 42). Therefore, it remains unclear which molecules and/or regulators are critical in the progress and restoration of tubular damage in CRF. On the basis of these findings, we focused on the M-phase regulators and then examined in vivo effects of a specific inhibitor for Cdc2 on their expression and renal function. The time-dependent expression profile of Cyclin B2-Cdc2 has been suggested to explain, in part, the balance of epithelial hypertrophy and hyperplasia in the remnant proximal tubules in progressive CRF.

MATERIALS AND METHODS

Animals. Male Wistar/ST rats (180–200 g) were subtotally nephrectomzed as described previously (17, 38). In brief, the right kidney was removed, and the posterior and anterior apical segmental branches of the left renal artery were individually ligated. Sham-operated rats at 2 wk after surgery were used as controls. Everolimus (LC Laboratories, Woburn, MA; 2 mg/kg body weight, E+), 2-cyanoethyl alsterpaullone [CE-ALP; Calbiochem, Darmstadt, Germany; 0.5 mg/kg body wt, dissolved in Cremophor-EtOH-DMSO-saline (12.5:12.5:5:70 vol/vol/vol/vol), A+], or vehicle (E− or A−) was subcutaneously administered to Nx rats every day for 2 wk after surgery. The animals were allowed free access to water and standard chow. To examine renal function, the levels of blood urea nitrogen (BUN) and plasma creatinine (PCr) and urine creatinine were determined. For measurements, we used an assay kit from Wako Pure Chemical Industries (Osaka, Japan). The urinary concentration of albumin was measured with an enzyme-linked immunosorbent

Address for reprint requests and other correspondence: Ken-ichi Inui, Dept. of Pharmacy, Kyoto University Hospital, Sakyo-ku, Kyoto 606-8507, Japan (e-mail: inui@kuhp.kyoto-u.ac.jp).

assay (ELISA) kit (Nephrat II, Exocell, Philadelphia, PA). For histological examinations, the kidney was stained with periodic acid Schiff (PAS) reagent by Sapporo General Pathology Laboratory (Hokkaido, Japan). The glomerular diameter and the height of epithelial cells were determined as mean values from 30 glomeruli and 20 proximal tubules in 3 rats, respectively. All protocols had been approved previously by the Animal Research Committee, Graduate School of Medicine, Kyoto University.

Isolation of proximal tubules by microdissection. To obtain renal proximal tubules, the rat nephron was microdissected as described previously (26). In brief, the left kidney was perfused and removed, and slices of the kidney were cut along the medullary axis and incubated with collagenase; the renal proximal tubules were then microdissected and isolated with sharp needles under a light microscope. After microdissection, the tubules (20 mm) were transferred into a microtube to isolate total RNA with the RNeasy mini kit (Qiagen, Hilden, Germany). The quality of total RNA was validated with a 2100 Bioanalyzer (Agilent Technologies, Santa Clara, CA). To examine the purity of isolated proximal tubules, RT-PCR and microarray analysis were performed with isolated proximal tubules and whole kidney specimens from normal rats (Supplemental Fig. S1).[1]

Microarray analysis using isolated proximal tubules. Digoxigenin (DIG)-UTP-labeled complementary (c)RNA was generated from the proximal tubular total RNA of four control rats (sham-operated rats at 2 wk after surgery) and Nx rats (1, 2, 4, and 8 wk after surgery) with Applied Biosystems Chemiluminescent RT-IVT Labeling Kit v2.0 (Applied Biosystems, Foster City, CA). Array hybridization, chemiluminescence detection, and image acquisition were performed according to the manufacturer's directions. In brief, 10 μg of cRNA was hybridized to Rat Genome Survey Microarrays (Applied Biosystems) at 55°C for 16 h. After the arrays were washed, anti-DIG-alkaline phosphatase (DIG-AP; Roche Diagnostic, Mannheim, Germany) was hybridized at room temperature for 20 min. Enhanced chemiluminescence signals were generated by adding the substrate solution and scanned with the ABI 1700 Chemiluminescent Microarray Analyzer (Applied Biosystems). The results of the microarray assay were analyzed with Spotfire software (TIBCO Software, Palo Alto, CA). After the bad spots were flagged, the assay signals were normalized across the experiments with each median. Furthermore, detectable signals were selected with a signal-to-noise (S/N) threshold (a gene with an S/N threshold >3 in 3 or 4 assays was considered to be detectable). The ratio of the signal from the Nx rat assay to the control signal was calculated, and a profile ANOVA was performed. Genes with a P value <0.01 and a ratio >2 or <0.5 were considered to be significantly upregulated or downregulated, respectively. Finally, these genes were classified with MetaCore Software (GeneGo, St. Joseph, MI) according to their function. A filled column in Fig. 1 indicates that the false discovery rate was <0.01.

Real-time PCR. Whole kidney total RNA was extracted with the MagNA Pure LC RNA Isolation Kit II (Roche Diagnostic). Total RNA was reverse transcribed with a High Capacity cDNA Reverse Transcription Kit (Applied Biosystems) and subjected to digestion with RNase H (Invitrogen, Carlsbad, CA). Real-time PCR was performed with the ABI PRISM 7900 Sequence Detection System (Applied Biosystems). The primer-probe set used for glyceraldehyde-3-phosphate dehydrogenase (GAPDH) and other genes were Predeveloped TaqMan Assay Reagents (Applied Biosystems) and

[1] The online version of this article contains supplemental material.

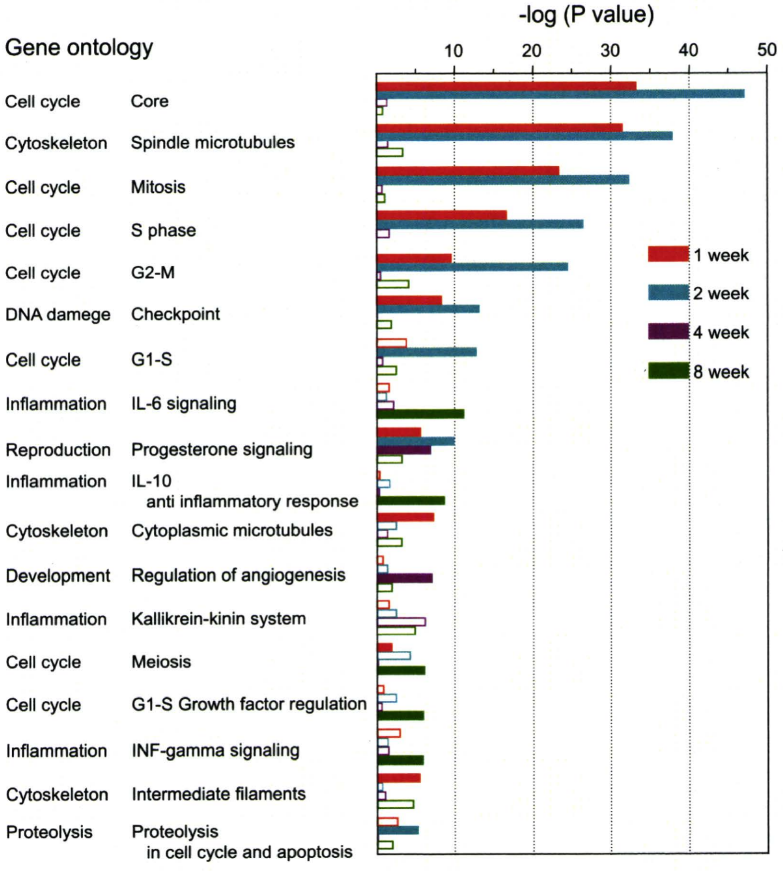

Fig. 1. Biological function of the genes significantly changed in the microarray analysis. To assess the results of the microarray analysis in terms of biological function, the genes that significantly changed each week after subtotal nephrectomy (Nx) were classified according to their Gene Ontology and P values were calculated with MetaCore software. A filled column implies that the false discovery rate was <0.01.

Table 1. *Biochemical parameters in sham-operated and subtotally nephrectomized rats*

		Nx			
	Sham (n = 10)	1 wk (n = 7)	2 wk (n = 13)	4 wk (n = 11)	8 wk (n = 9)
Body weight, g	264.1 ± 6.2	210.7 ± 6.0†	231.5 ± 5.9*	288.4 ± 7.7	323.9 ± 12.2†
Urine volume, ml/day	6.9 ± 1.0	24.8 ± 1.9†	23.6 ± 1.7†	26.4 ± 1.8†	25.3 ± 3.4†
BUN, mg/dl	13.5 ± 0.5	44.1 ± 6.5	57.4 ± 6.5†	71.0 ± 12.0†	85.0 ± 15.3†
PCr, mg/dl	0.52 ± 0.02	1.22 ± 0.18*	1.23 ± 0.10*	1.26 ± 0.15*	1.96 ± 0.32†
CCr, $ml \cdot min^{-1} \cdot kg^{-1}$	4.42 ± 0.23	2.70 ± 0.36†	2.31 ± 0.22†	2.46 ± 0.28†	1.69 ± 0.30†
Albumin excretion, mg/day	0.5 ± 0.1	3.5 ± 0.3	21.5 ± 4.7	67.4 ± 4.5*	128.6 ± 45.2†

Data represent means ± SE for n rats. Sham, sham-operated rats at 2 wk after surgery; Nx, 5/6 nephrectomized rats; BUN, blood urea nitrogen; PCr, plasma creatinine; CCr, creatinine clearance. Multiple comparison was performed with Dunnett's 2-tailed test after a 1-way ANOVA. *$P < 0.05$, †$P < 0.01$, significantly different from Sham.

Premade TaqMan Assay Reagents, respectively. GAPDH mRNA expression was measured as an internal control.

Measurement of Cdc2 activity in kidney. The activities of Cdc2 in the kidney were examined with the MESACUP cdc2 Kinase Assay Kit (MBL, Nagoya, Japan) according to the manufacturer's instructions with slight modification. The kidney was homogenized in lysis buffer [in mM: 50 Tris · HCl pH 7.5, 150 NaCl, 10 NaF, 1 $Na_4P_2O_7$, and 100 Na_3VO_4, with 1% NP-40, 1% protease inhibitor cocktail (Nacalai Tesque, Kyoto, Japan), and phosphatase inhibitor (PhosSTOP; Roche Diagnostic)]. The tissue lysate was clarified by centrifugation, and protein concentrations were determined with the Bradford protein assay. The phosphorylation reaction was performed with the lysate (50 μg) in the presence of 0.1 mM ATP at 30°C for 5 min. The phosphorylated substrates were detected by ELISA.

In situ hybridization. Fixed paraffin-embedded blocks and sections of rat kidney for in situ hybridization were obtained from Genostaff (Tokyo, Japan). After dewaxing and rehydration, the sections (6 μm) were fixed with 4% paraformaldehyde. The sections were treated with proteinase K, washed with PBS, and placed in 0.2 N HCl for 10 min. After washing, the sections were acetylated by incubation in 0.1 M triethanolamine-HCl and 0.25% acetic anhydride for 10 min. Hybridization was performed with probes specific for Cyclin B2 and Cdc2 (300 ng/ml) at 60°C for 16 h. The sections were then washed in HybriWash (Genostaff) before being subjected to RNase treatment. After treatment with 0.5% blocking reagent (Roche Diagnostic), the sections were incubated with anti-DIG-AP conjugate (Roche Diagnostic) for 2 h. Coloring reactions were performed with nitro blue tetrazolium chloride-5-bromo-4-chloro-3-indolyl phosphatase (NBT-BCIP; Sigma-Aldrich, St. Louis, MO) overnight. They were then counterstained with Kernechtrot stain solution.

Immunofluorescent analysis. The fixed tissue sections were prepared and immunofluorescent analysis was performed as described previously with slight modification (29, 30). The animals were anesthetized, and the kidneys were perfused via the abdominal aorta, first with saline containing 50 U/ml of heparin and then with 4% paraformaldehyde in PBS. Fixed tissues were embedded in Tissue-Tek OCT compound (Sakura Finetek, Tokyo, Japan) and frozen rapidly in liquid nitrogen. Sections (5 μm thick) were cut and covered with 5% BSA and 0.3% Triton X-100 in PBS for Ki-67, rabbit serum (Invitrogen) for Cyclin B2, and SuperBlock Blocking Buffer (Thermo Fisher Scientific, Waltham, MA) for Cdc2 at 37°C for 60 min. The covered

Table 2. *Number of genes in microarray analysis*

	1 wk	2 wk	4 wk	8 wk
Total number	239	161	278	389
Up/down	191/48	79/82	176/102	268/117
Unique number	103	37	121	246
Up/down	98/5	24/13	97/24	206/40
Common number			36	
Up/down			3/33	

Sham-operated rats at 2 wk after surgery were used as controls. Genes were selected when the ratio to control was >2 or <0.5 and the P value was <0.01. Unique and common imply that the genes specifically changed in each week and throughout the experimental period, respectively.

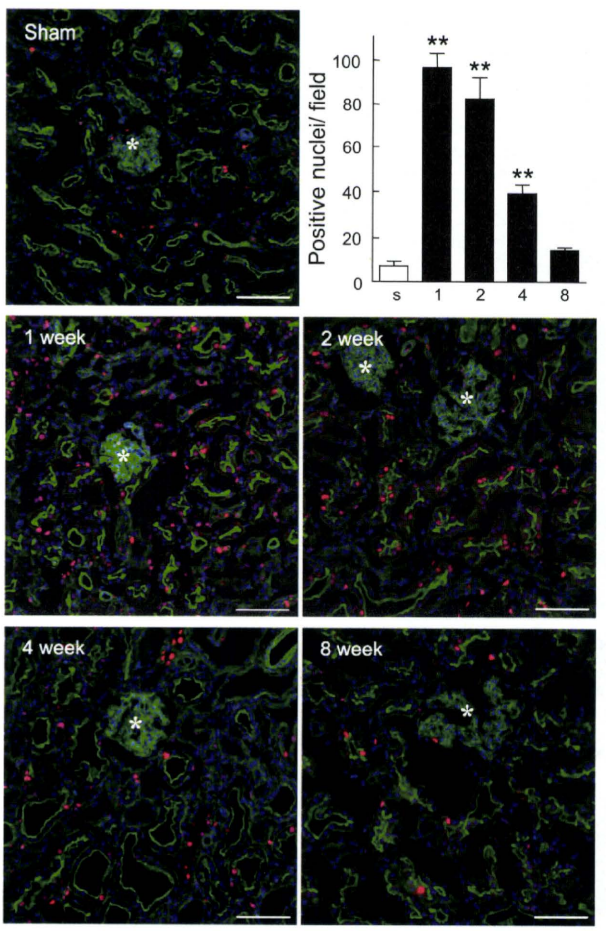

Fig. 2. Expression of Ki-67 in the kidney. Immunofluorescent labeling of Ki-67 in sham-operated and Nx rats at 1, 2, 4, and 8 wk after surgery is shown. Red signals for Ki-67 merged with green signals for phalloidin and with blue signals for 4′,6-diamidino-2-phenylindole (DAPI). *, Glomeruli. Scale bars 100 μm. Stained nuclei in the proximal tubules were counted in 3 independent regions at 100-fold magnification. s, Sham-operated rats; 1, 2, 4, and 8, Nx rats at 1, 2, 4, and 8 wk after surgery. Multiple comparisons were performed with Dunnett's 2-tailed test after a 1-way ANOVA. **$P < 0.01$, significantly different from sham-operated rats.

sections were incubated with antiserum specific for Ki-67 (1:500; Abcam, Cambridge, UK), Cyclin B2 (1:200, Abcam), and Cdc2 (1:200, Cell Signaling Technology, Danvers, MA) at 4°C overnight. After further washing, the sections were incubated with Alexa Fluor 546-labeled goat anti-rabbit IgG or Alexa Fluor 488-labeled anti-mouse IgG, Alexa Fluor 488-labeled phalloidin or Alexa Fluor 594-labeled phalloidin (Invitrogen), and 4′,6-diamidino-2-phenylindole (DAPI; Wako) at 37°C for 60 min.

Immunohistochemistry of phospho-histone H3 at serine 10. The sections of immunohistochemistry were obtained from Genostaff. After deparaffinization and rehydration, the sections (5 μm) were treated with proteinase K and 0.3% hydrogen peroxide. The sections were blocked with Protein Block (Dako) and the Avidin/Biotin Blocking Kit (Vector Laboratories, Burlingame, CA) followed by incubation with anti-phospho-histone H3 (serine 10) (p-histone H3) antibody (Abcam) at 4°C overnight. After washing, the sections were incubated with biotinylated goat anti-rabbit IgG (Dako). After further washes, the sections were incubated with an avidin-biotinylated horseradish peroxidase complex (Nichirei Biosciences, Tokyo, Japan). Coloring reactions were performed with hydrogen peroxide containing 3,3′-diaminobenzidine (DAB-H_2O_2). The sections were then counterstained with hematoxylin stain solution.

Image analysis. The images of in situ hybridization and immunofluorescent and immunohistochemical analysis were captured and examined with BZ-9000 (Keyence, Osaka, Japan). To evaluate the levels of Ki-67, Cyclin B2, Cdc2, and p-histone H3, three or six independent photographs in the renal cortex were taken at 100-fold magnification (each total area 1.58 μm^2), and the stained nuclei in the proximal tubules were counted.

Statistical analysis. All data are expressed as means ± SE. Comparisons were performed with the unpaired *t*-test. Multiple comparisons were performed with a one-way ANOVA. Probability values of <0.05 were considered statistically significant.

RESULTS

Gene expression profile of renal proximal tubules in CRF rats. Before microarray analyses were performed with the isolated proximal tubules, the purity of the proximal tubules was examined by RT-RCR (Supplemental Fig. S1*A*). The band

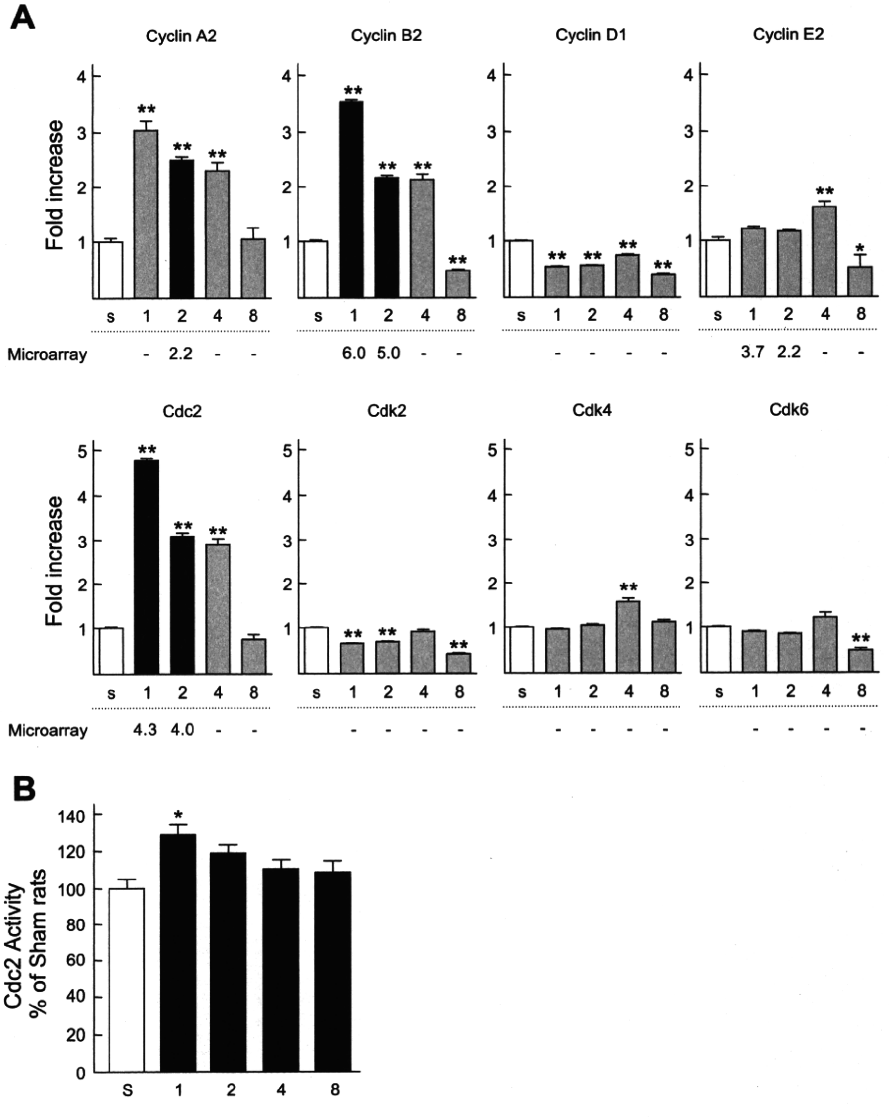

Fig. 3. Expression levels of cell cycle-related genes and the activities of Cell division cycle 2 (Cdc2) in the remnant kidney. *A*: mRNA levels of Cyclin A2, Cyclin B2, Cyclin D1, Cyclin E2, Cdc2, Cyclin-dependent kinase (Cdk)2, Cdk4, and Cdk6. An equal amount of cDNA was pooled from the remnant kidney of each rat, and the expressional changes of mRNA were measured by real-time PCR and analyzed by the $\Delta\Delta C_t$ method (where C_t is threshold cycle). Numbers below each column show the fold change in the microarray analysis; − indicates that expressional change was not significant in the microarray analysis. Open columns represent levels in sham-operated rats; black and gray columns represent results of the microarray analysis validated by real-time PCR analysis or not, respectively. *B*: kinase activities of Cdc2. Multiple comparisons were performed with Dunnett's 2-tailed test after a 1-way ANOVA. $*P < 0.05$, $**P < 0.01$, significantly different from sham-operated rats.

for Na^+-glucose cotransporter (SGLT)2, a marker for proximal tubules (46), was clearly found in the proximal tubules, while those for podocin, Na^+-K^+-Cl^- cotransporter (NKCC)2, and aquaporin (AQP)-2, markers for glomeruli (18), thick ascending limbs (8), and collecting ducts (7), respectively, were not amplified in the proximal tubules, whereas all bands were found in the whole kidney. Simultaneously, the expressional profiles in the isolated proximal tubules and whole kidney were compared by microarray analysis (Supplemental Fig. S1*B*). Consistent with the results of RT-PCR, the intensity of SGLT2 in the proximal tubules was much higher than in whole kidney. On the other hand, the genes that were not contained in the proximal tubules such as hemoglobin showed low intensity in the proximal tubules. Consequently, the purity of the isolated proximal tubules was well confirmed.

After Nx, urine volume and PCr significantly increased, BUN and urinary albumin excretion time-dependently increased, and creatinine clearance (CCr) markedly decreased compared with sham-operated rats (Table 1). Therefore, marked renal insufficiency and its progression were confirmed in Nx rats. Next, microarray analyses were performed with isolated renal proximal tubules of these sham-operated and Nx rats. To establish distinctive expressional profiles of proximal tubules in progressive CRF, genes were selected according to the criteria described in MATERIALS AND METHODS. The numbers of selected genes after statistical analysis are summarized in Table 2. Among these, the total numbers of genes whose expression was significantly changed more than twofold compared with control at 1, 2, 4, and 8 wk after surgery were 239, 161, 278, and 389, respectively. On the basis of the total number of genes, we classified them according to their Gene Ontology, using MetaCore software to identify the biological function involved in the progression of CRF in the proximal tubules. The results revealed that the cell cycle- or cytoskeleton-related genes were significantly altered at 1 and 2 wk after Nx (Fig. 1). On the other hand, inflammation-related genes were frequently detected at 8 wk after Nx.

Validation of microarray analysis revealed activation of mitosis-specific genes in remnant kidney immediately after Nx. To examine whether renal epithelial cells entered into the cell cycle immediately after Nx, the expression of Ki-67, a proliferation marker (9), was examined. Comparable to the results of microarray analysis, the proximal tubules of Nx rats at 1, 2, and 4 wk after surgery showed abundant staining for Ki-67 compared with those in the sham-operated rats; however, the number of stained nuclei in the proximal tubules was markedly decreased to approximately control level at 8 wk after surgery (Fig. 2). Furthermore, the mRNA levels of some cell cycle regulators were examined by real-time PCR using cDNA of the remnant kidney to confirm whether the expression of these genes was also detected in whole kidney samples. Among eight cell cycle-related genes such as Cyclins (Cyclin A2, B2, D1,

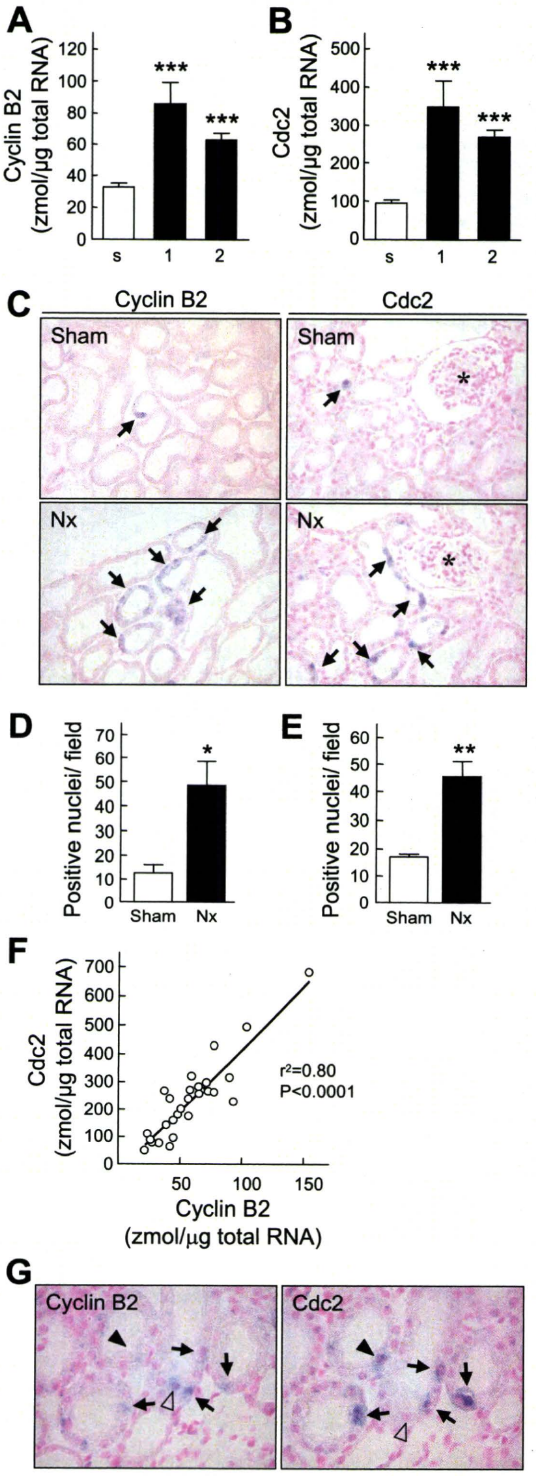

Fig. 4. Detection of Cyclin B2 and Cdc2 in the kidney by real-time PCR and in situ hybridization analysis. *A* and *B*: mRNA levels of Cyclin B2 (*A*) and Cdc2 (*B*) were measured by real-time PCR. s, Sham-operated rats; 1 and 2, Nx rats at 1 and 2 wk after surgery. Multiple comparisons were performed with Dunnett's 2-tailed test after a 1-way ANOVA. ***$P < 0.001$, significantly different from sham-operated rats. *C*: in situ hybridization of Cyclin B2 (*left*) and Cdc2 (*right*). *, Glomeruli. Magnification ×200. *D* and *E*: Cyclin B2 (*D*)- and Cdc2 (*E*)-positive nuclei in the renal cortex were counted. *$P < 0.05$, **$P < 0.01$, significantly different from sham-operated rats. *F*: correlation between mRNA levels of Cyclin B2 and Cdc2. Linear regression analysis was performed, and the correlation coefficient (r) was calculated. *G*: in situ hybridization analysis of Cyclin B2 and Cdc2 with serial sections in Nx rats was carried out. Arrows, positive staining for both Cyclin B2 and Cdc2; open arrowhead, positive staining for Cyclin B2 without Cdc2; filled arrowhead, positive staining for Cdc2 without Cyclin B2.

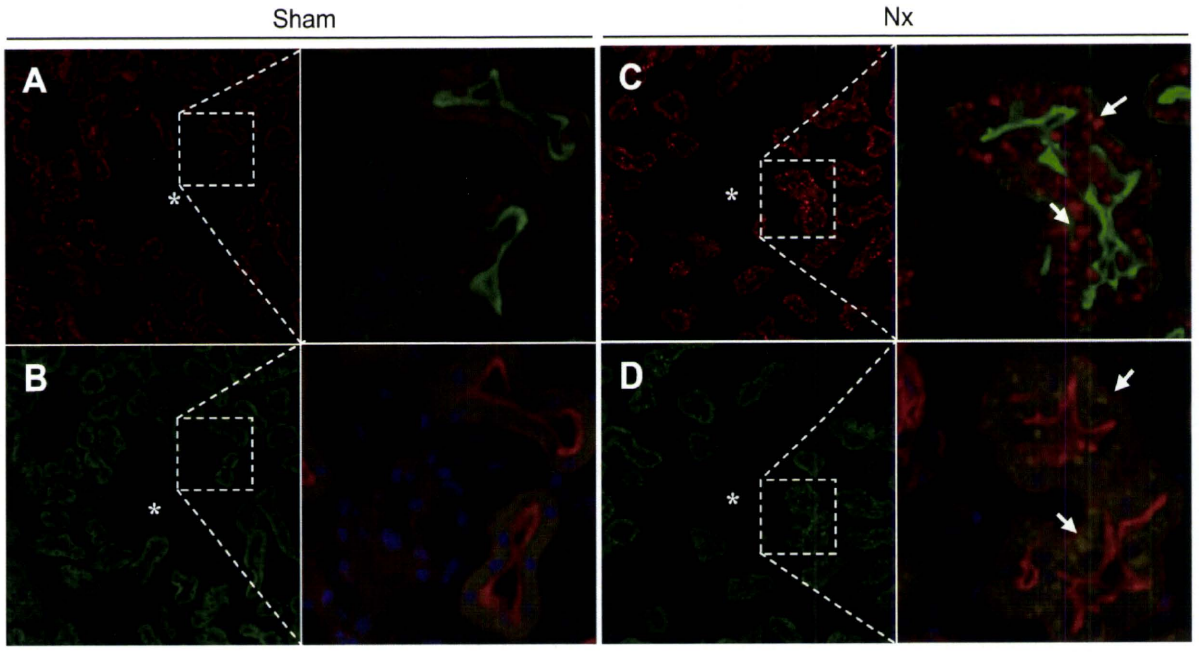

Fig. 5. Immunofluorescent analysis of Cyclin B2 and Cdc2 in the kidney. The kidney was perfused, fixed, and then embedded. Sections (5 μm) were stained with a specific antibody for Cyclin B2 (*A* and *C*, red) or Cdc2 (*B* and *D*, green), phalloidin (*A* and *C*, green; *B* and *D*, red), and DAPI (blue). *A* and *B*: series of sections from sham-operated rat kidney. *C* and D: series of sections from Nx rat kidney at 2 wk after surgery. Arrows, aggregation of signals for Cyclin B2 or Cdc2; *, glomeruli. Magnification ×200 and ×400.

and E2) and Cyclin-dependent kinases (Cdk; Cdk2, 4, 6 and Cdc2), the changes in the levels of Cyclin B2 and Cdc2 at 1 and 2 wk after Nx corresponded well with the results of the microarray analysis (Fig. 3*A*). The activities of Cdc2 were significantly increased in Nx rats at 1 wk after surgery compared with sham-operated rats, and the increased activity was retained at 2 wk after Nx (Fig. 3*B*). Furthermore, Cdc2 activity was decreased almost to the sham-operated level with the progression of CRF.

Cyclin B2 and Cdc2 were specifically expressed and upregulated in renal proximal tubules of CRF rats. On the basis of the validation of microarray analysis and the enhancement of Cdc2 activity in the remnant kidney, we focused on Cyclin B2 and Cdc2 and further confirmed the expression of these genes in individual sham-operated and early-stage Nx rats. The mRNA levels of Cyclin B2 and Cdc2 were significantly increased in the remnant kidney at 1 and 2 wk after Nx compared with the sham-operated rats (Fig. 4, *A* and *B*). On the basis of the in situ hybridization analysis, the mRNAs of Cyclin B2 and Cdc2 were specifically visualized in a portion of the epithelial cells in the proximal tubules in sham-operated rats, and their expression levels were markedly increased in the proximal tubules of Nx rats at 2 wk after surgery (Fig. 4*C*, arrows). The number of stained nuclei in the proximal tubules of renal cortex significantly increased to approximately threefold in the Nx rats, which was consistent with the results of real-time PCR (Fig. 4, *D* and *E*). We examined the relationship between the levels of Cyclin B2 and Cdc2 because both proteins function as heterodimers in the mitotic phase (16). The mRNA level of Cyclin B2 correlated well with that of Cdc2 (coefficient of correlation $r^2 = 0.80$, $P < 0.0001$) (Fig. 4*F*). Furthermore, most of the signals for Cyclin B2 and Cdc2 were simultaneously observed in the proximal tubular cells (Fig. 4*G*, arrows), and a portion of them were independently detected (Fig. 4*G*, open and filled arrowheads).

On immunofluorescent analysis with serial sections, Cyclin B2 and Cdc2 signals were slightly detected in the proximal tubules, but no signals were observed at the glomeruli or other tubular segments in the sham-operated rats (Fig. 5, *A* and *B*). In Nx rats, Cyclin B2 and Cdc2 signals were markedly increased and aggregated in the proximal tubules (Fig. 5, *C* and *D*). As indicated by in situ hybridization, the localization of Cyclin B2 and Cdc2 was identified in the same epithelial cells (Fig. 5, *C* and *D*, arrows).

Effects of mammalian target of rapamycin inhibitor in CRF rats. Next, we examined the effects of the mammalian target of rapamycin (mTOR) inhibitor everolimus on the expression levels of Cyclin B2 and Cdc2 and renal function of Nx rats at 2 wk after surgery. Everolimus markedly reduced the mRNA expression of Cyclin B2 and Cdc2 in Nx rats to levels similar to those in sham-operated rats (Fig. 6, *A* and *B*, vs. Fig. 4, *A* and *B*). Immunofluorescent analysis revealed that Ki-67-positive proximal tubular epithelial cells were decreased to 20% in everolimus-treated (E+) rats compared with those in vehicle-treated (E−) rats (Fig. 6, *C* and *D*). As shown in Fig. 6*E*, compensatory renal hypertrophy was significantly inhibited by the administration of everolimus. Correspondingly, the kidney-to-body weight ratio was significantly decreased by everolimus treatment, although the body weight of these rats was markedly decreased compared with that of the vehicle-treated rats (Table 3, E− vs. E+). Histological examination of the remnant kidneys also showed inhibition of glomerular and tubular hypertrophy in E+ rats (Fig. 6*F*). Moreover, the glomerular diameter and height of epithelial cells were significantly decreased in E+

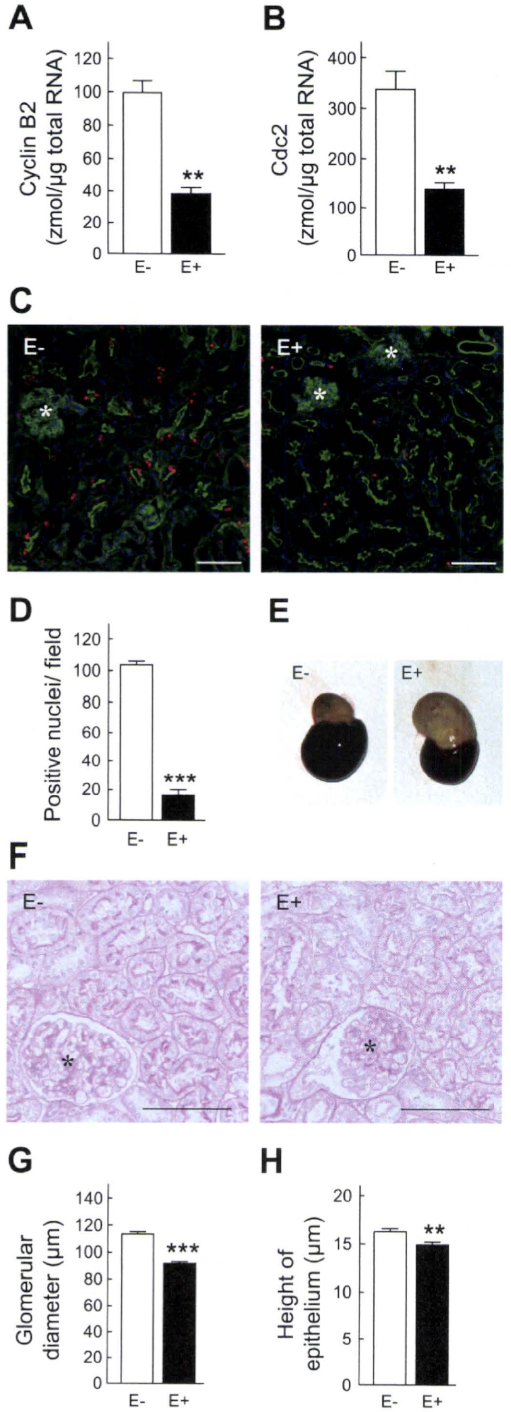

Fig. 6. Effects of administration of everolimus in Nx rats. Nx rats were subcutaneously treated with vehicle (E−) or everolimus (E+, 2 mg/kg) for 14 days immediately after Nx. *A* and *B*: detection of mRNA of cyclin B2 (*A*) and Cdc2 (*B*) by real-time PCR. *C*: immunofluorescent analysis of Ki-67. *D*: numbers of stained nuclei for Ki-67 in the proximal tubules were counted in 3 independent regions at 100-fold magnification. *E*: appearance of remnant kidney. *F*: representative photographs of periodic acid Schiff (PAS) staining of the remnant kidney. *G* and *H*: measurement of glomerular diameter (*G*) and the height of epithelial cells (*H*). *, Glomeruli. Scale bars 100 μm. $^{**}P < 0.01$, $^{***}P < 0.001$, significantly different from vehicle-treated (E−) rats.

rats (Fig. 6, *G* and *H*). At this time, administration of everolimus markedly increased the level of BUN and PCr and decreased the level of CCr (Table 3). However, urinary excretion of albumin was lowered in the E+ rats to ~30% of that in the E− rats.

Effect of Cdc2 inhibitor in CRF rats. A Cdc2-specific inhibitor, CE-ALP, was administered to Nx rats to obtain more direct information about the significance of cell cycle-related molecules during the compensative period. The mRNA levels of Cyclin B2 and Cdc2 showed no difference with or without administration of the inhibitor (Fig. 7, *A* and *B*). However, administration of CE-ALP significantly decreased the number of nuclei with positive signals for Ki-67 to ~60% in the proximal tubules (Fig. 7, *C* and *D*). CE-ALP also deteriorated renal function of Nx rats, although the effects were less than those of everolimus. The level of BUN was significantly increased, the urine volume and PCr were also increased, and CCr was decreased in the CE-ALP-treated rats (Table 3, A− vs. A+). The excretion of albumin tended to be high, suggesting that the kidney was further damaged by Cdc2 inhibition. Histological examination of the remnant kidneys revealed that the glomerular diameter was not affected, but the height of epithelial cells was significantly increased by the treatment with CE-ALP (Fig. 7, *E–G*).

Effects of everolimus and CE-ALP on expression of p-histone H3 and activity of Cdc2. To examine whether renal proximal tubular cells underwent mitosis in compensative CRF, the levels of p-histone H3, a mitosis marker (12), were examined and the positive nuclei were counted (Fig. 8, *A* and *B*). p-Histone H3 staining in the proximal tubular nuclei was abundantly observed in Nx rats compared with sham-operated rats. Administration of everolimus abolished the level of p-histone H3 almost to the level of the sham-operated rats. In addition, treatment with CE-ALP clearly decreased the level of p-histone H3 to ~50% in Nx rats. Consistent with the immunohistochemical analysis of p-histone H3, the activities of Cdc2 after the administration of everolimus and CE-ALP were significantly decreased compared with those of the vehicle-treated Nx rats (Fig. 8*C*).

DISCUSSION

The kidney is a heterogeneous organ with many types of cells; therefore, it is difficult to clarify the cell-specific changes in molecular events in CRF. Almost no microarray analyses have been undertaken with nephron segment-selective samples. In statistical analyses of microarray experiments, strong expression signals derived from other segments often disturb the detection of responses in intact proximal tubular epithelial cells. Previous gene expression profiles focusing on tubular cells were obtained with rat primary proximal tubular cells (36, 41) or human proximal tubule-derived HK-2 cells (22) to study the responses to nephrotoxic drugs or hypoxia. Therefore, these previous reports could not explain the pathophysiology of progressive CRF in vivo. The present study was designed to investigate these issues by continuously isolating viable proximal tubules during CRF progression. The histology of the remnant kidneys showed severe glomerular sclerosis, tubular dilation, and interstitial fibrosis at 4–8 wk after Nx (Supplemental Fig. S2*A*). The accumulation of ED1 (a marker of infiltrated macrophage) and α-smooth muscle actin (a fibrotic marker) was also observed in the later phase of Nx rats

Table 3. *Effects of administration of everolimus and Cdc2 inhibitor on renal function in Nx rats*

	Everolimus		2-Cyanoethyl Alsterpaullone	
	E− (n = 8)	E+ (n = 6)	A− (n = 11)	A+ (n = 9)
Body weight, g	226.1 ± 5.3	171.9 ± 4.5‡	242.5 ± 3.6	222.7 ± 8.8*
Kidney weight/body weight, %	0.26 ± 0.01	0.22 ± 0.01†	0.24 ± 0.01	0.24 ± 0.01
Urine volume, ml/day	15.4 ± 1.8	17.7 ± 3.9	25.3 ± 2.0	29.1 ± 2.3
BUN, mg/dl	41.9 ± 4.8	68.1 ± 5.0†	39.2 ± 2.0	54.2 ± 7.2*
PCr, mg/dl	0.90 ± 0.07	1.17 ± 0.08†	1.07 ± 0.05	1.22 ± 0.01
CCr, $ml \cdot min^{-1} \cdot kg^{-1}$	2.83 ± 0.17	1.41 ± 0.16‡	2.69 ± 0.19	2.44 ± 0.27
Albumin excretion, mg/day	8.4 ± 4.5	2.4 ± 1.0	5.7 ± 1.5	11.8 ± 3.9

Data represent means ± SE for n rats. E− and A−, Nx rats administered vehicle; E+ and A+, Nx rats daily administered everolimus (2 mg/kg) and 2-cyanoethyl alsterpaullone (0.5 mg/kg) for 14 days, respectively. *$P < 0.05$, †$P < 0.01$, ‡$P < 0.001$, significantly different from vehicle-treated rats.

(Supplemental Fig. S2, *D* and *E*). However, the molecules related to the fibrotic response, such as transforming growth factor-β or connective tissue growth factor (2, 5), were not increased in the microarray analysis of proximal tubules even 8 wk after Nx. Furthermore, interleukin-1β and tumor necrosis factor-α were also undetectable, although they were reported to be increased in Nx rats in a study using whole kidney samples (37). Therefore the present microarray data may be considered to accurately reflect the responses to CRF in the proximal tubules, avoiding contamination from other nephron segments and infiltrating immune cells.

Immediately after Nx, significant changes were found in the expression of cell cycle-related genes (Fig. 1). The mammalian cell cycle is positively regulated by complexes of cell cycle proteins consisting of a catalytic subunit (called Cdk) and a regulatory subunit (called cyclin). In addition, the cyclin-Cdk complexes are negatively regulated by proteins called Cdk inhibitors (10). Several studies showed that cell cycle regulators are involved in renal pathophysiology. In acute renal injury, it is considered that cell cycle activation focusing on Cdk2 and Cdk inhibitor $p21^{WAF1/Cip1}$ contributes to both cellular life and death in the renal tubules (31). Megyesi et al. (27) reported that $p21^{WAF1/Cip1}$-knockout mice did not develop CRF such as glomerular sclerosis and systemic hypertension. However, there is no clear difference in renal function between the presence and absence of $p21^{WAF1/Cip1}$ immediately after renal ablation. In the present study, the increase in expression of $p21^{WAF1/Cip1}$ was found in both microarray analysis and real-time PCR and the enhancements were retained throughout the experimental period (Supplemental Fig. S3). Furthermore, $p21^{WAF1/Cip1}$ affects several phases of the cell cycle through the inhibition and interaction of Cdks (43). On the basis of these results and reports, further study might be needed to clarify the specific contribution of $p21^{WAF1/Cip1}$ to compensative CRF.

It is reported that the renal hypertrophy is modulated by a cell cycle-dependent mechanism whereby Cyclin D-Cdk4/6 is activated without subsequent Cyclin E-Cdk2 involvement; thus the cell cycle is arrested in late G_1, resulting in cellular hypertrophy (23, 33). Other studies have demonstrated that the induction and accumulation of Cdk inhibitor $p27^{Kip1}$ play pivotal roles in the arrest in G_1 by using an in vitro model of hypertrophy (42). Considering the expression profiles, the levels of D-type cyclins, E-type cyclins, Cdk2, Cdk4, Cdk6, as well as $p27^{Kip1}$ were not definitively changed in the compensatory period in Nx rats because of the lowered fold changes or S/N threshold. In contrast, the expression of Cyclin B2 and Cdc2, which mediated the M-phase transition, was significantly upregulated and the activities of Cdc2 were increased in the remnant kidney, especially at early stages (Fig. 3). Furthermore, the two were colocalized to the same epithelial cells in Nx rats (Figs. 4*G* and 5, *C* and *D*). It is known that two B-type cyclins (B1 and B2) are able to bind and activate Cdc2. We also examined the level of Cyclin B1, although statistically significant changes were not observed in the microarray analysis (Supplemental Fig. S4). Interestingly, the expression pattern after Nx and response to everolimus in Cyclin B1 was quite similar to those in Cyclin B2 and Cdc2. These results clearly indicated the coordination of their functions and the activation of a state of M phase in the epithelial cells in the Nx rat kidneys.

Among five Cdks, only disruption of Cdc2 caused embryonic lethality in the studies with gene knockout mice, indicating that the G_2-M regulator is a crucial factor in embryonic development (32). We confirmed that the mRNA levels of Cdc2 as well as Cyclin B1 and B2 were high during renal development and decreased with growth (Supplemental Fig. S5, *A–C*). Furthermore, the activities of Cdc2 were well correlated with the mRNA levels of Cdc2 ($r^2 = 0.86$, $P < 0.0001$), suggesting that the mRNA level might reflect the activity of Cdc2 (Supplemental Fig. S5*D*). Thus the M-phase regulator Cdc2, in association with Cyclin B, is essential for the promotion of the cell cycle, and we suggest that these regulators are responsible for compensative proliferation of the proximal tubular epithelium itself. On the contrary, the expression levels of Cyclin B2 and Cdc2 and the activity of Cdc2 in the remnant kidney were reduced almost to the sham-operated level, and the Ki-67-positive tubules were markedly decreased at 8 wk after surgery. These phenomena might be associated with the expression profile of Cyclin B-Cdc2 in that the epithelial cells in the fibrotic period could not proliferate because of the lack of M-phase cyclins. Several reports demonstrated that the mitotic cyclins were mainly regulated at the level of transcription by some transcriptional factors such as B-MYB, E2F, FOXM1, and NF-Y (6). In the present study, the expression of these transcriptional factors was not significantly changed by Nx treatment in the microarray analysis, and therefore further examinations would be needed to clarify the molecular mechanisms of the increase in Cyclin B2-Cdc2 after Nx.

The mTOR pathway has been demonstrated to contribute to the tissue hypertrophy (21) and pathophysiology of several kidney diseases such as diabetic nephropathy (24, 45) and polycystic kidney disease (34, 39). Treatment with the mTOR inhibitor rapamycin (sirolimus) was reported to attenuate renal